PHOTOELECTRIC EMISSION MEASUREMENTS FOR CVD GROWN POLYCRYSTALLINE DIAMOND FILMS

Tarek Hassan, B.Sc.

Problem in Lieu of Thesis Prepared for the Degree of

MASTER OF SCIENCE

UNIVERSITY OF NORTH TEXAS

August 1999

APPROVED:

Jose M. Perez, Major Professor
Zhibing Hu, Committee Member
David Shiner, Committee Member
Duncan Weathers, Coordinator of the program in Physics
Sam Matteson, Chair of the Department of Physics
C. Neal Tate, Dean of the Robert B. Toulouse School of Graduate Studies

Hassan, Tarek, Photoelectric Emission Measurements for CVD Grown Polycrystalline Diamond Films. Master of Science (Physics), August 1999, 63 pp., 6 tables, 34 illustrations, References, 22 titles.

We examined CVD grown polycrystalline diamond films having different methane concentrations to detect defects and study the possible correlation between the methane concentration used during the growth process and the defect density. SEM and Raman results show that the amorphous and sp^2 carbon content of the films increases with methane concentration. Furthermore, photoelectric emission from diamond is confirmed to be a two-photon process, hence the electrons are emitted from normally unoccupied states. We found that the photoelectric yield, for our samples, decreases with the increase in methane concentration. This trend can be accounted for in two different ways: either the types of defects observed in this experiment decrease in density as the methane concentration increases; or, the defect density stays the same or increases, but the increase in methane concentration leads to an increase in the electron affinity, which reduces the overall photoelectric yield.

TABLE OF CONTENTS

LIST OF TABLES

LIST OF ILLUSTRATIONS

CHAPTER 1

INTRODUCTION

Diamond is known to be one of the most attractive gems because of its unique structure which makes diamond gems have many reflective surfaces, thus making it ideal for jewelry. In addition to its esthetic values, diamond is a very attractive technological material because of its unique combination of properties. “Choose virtually any characteristic property of a material--structural, electrical or optical--and the value associated with diamond will almost always represent an extremist position among all materials considered for that property” [1]. Some of the long-known unique properties of diamond are listed qualitatively below.

- Hardest known material
- Best thermal conductor of any material near room temperature
- Resistant to heat, acids, and radiation
- Good electrical insulator, but can be doped to form p- and n-type semiconductors
- Highest figure of merit for power semiconductor applications
- Transparent to visible and infrared radiation
- Small dielectric constant

This combination of properties make diamond very appealing for industrial applications. Some of the traditional applications are heat sinks, high power and high temperature semiconductor devices, and coatings on cutting tools and bearings. Some of the properties of diamond are listed in table 1. Table 2 compares some of the electrical properties of diamond with two common semiconductors: GaAs and Si [1].

Although bulk diamond has many interesting properties, it is impossible to effectively engineer it into the various physical configurations required to exploit all the desired combinations of these properties. Only with the advent of the chemical vapor deposition (CVD) synthesis technique, allowing the growth of diamond films and coatings, has diamond become an engineered material that is now part of many industrial applications. CVD is based on the activated decomposition of gaseous molecules such as methane, acetylene, or carbon monoxide. This method now makes available for the first time the high-performance properties of diamond over large areas and in a variety of unique shapes and forms not available from nature or from the high-pressure-high-temperature (HPHT) diamond synthesis method [1].

Moreover, the recent discovery of negative electron affinity (NEA) in CVD grown diamond films opened yet another avenue in the applications of diamond utilizing its field emission properties [1]. A lot of work has been done in the last few years on the field emission properties of diamond films because of their promising industrial applications. Examples of these applications currently under investigation are flat panel displays, secondary electron emitters, and ultraviolet photo-cathode detectors. Unfortunately, the process by which diamond films field-emit is still unknown. However, some of the studies done on diamond films have shown that field emission

Table 1. Properties of diamond.

Property	Value	Units
Hardness	$1.0x10^{14}$	Kg/mm^2
Strength, tensile	>1.2	GPa
Strength, compressive	>110	GPa
Coefficient of friction (Dynamic)	0.03	Dimensionless
Sound velocity	$1.8x10^4$	m/s
Density	3.52	g/cm^3
Young's modulus	1.22	GPa
Thermal expansion coefficient	$1.1x10^{-6}$	K^{-1}
Thermal conductivity	20.0	W/cm.K
Debye temperature	2200	K
Optical index of refraction (at 591 nm)	2.41	Dimensionless
Optical transmissivity (from nm to far IR)	225	Dimensionless
Dielectric constant	5.7	Dimensionless
Dielectric strength	$1.0 x10^7$	V/cm
Electron mobility	2200	$cm^2/V.s$
Hole mobility	1600	$cm^2/V.s$
Electron affinity	Negative	eV
Bandgap	5.45	eV
Resistivity	10^{13}-10^{16}	Ω.cm

Table 2. Electrical properties of diamond v. GaAs and Si.

Property	Diamond	GaAs	Si	Unit
Bandgap	5.45	1.43	1.1	eV
Hole mobility	1800	400	600	$cm^2/V.s$
Electron mobility	2000	8500	1500	$cm^2/V.s$
Resistivity	10^{16}	10^9	10^3	Ω.cm
Dielectric constant	5.7	12.5	11	Dimensionless
Dielectric strength	10	6	5	V/cm x 10^6
Electron affinity	Negative	2.0	2.0	eV
High field electron velocity	2.7	1	1	cm/s x 10^7

increases with the increase in methane concentration used during growth. Moreover, these studies have hypothesized that higher methane concentration causes higher defect density, suggesting that field emission in diamond films is due to defects.

This experiment studies polycrystalline diamond films grown using chemical vapor deposition (CVD). It has two goals. First, detect the existence of defects that relate to trapping or emission of electrons by measuring photoelectric emission. Second, study the possible correlation between methane concentration and defect density by studying the behavior of photoelectric emission as the methane concentration changes. Raman spectroscopy is used for the characterization of the sp^2/sp^3 carbon content of the sample and a microchannel plate is used to measure photoelectric emission. What is unique about the setup used in this experiment is that the Raman spectroscopy and photoelectric emission measurements are done simultaneously using a confocal optical system. Also,

scanning electron microscopy (SEM) is used to study the morphology of the diamond films. The results of this experiment help understand the types of defects in diamond films and to what extent defects contribute to field emission from diamond films.

CHAPTER 2

EXPERIMENTAL SETUP

The goal of this chapter is to discuss the apparatus and experimental techniques used in this experiment. I will first give a general discussion of each technique. Then, in the last section of this chapter I will discuss the specific setup used in this experiment. Three different experimental techniques are used in this experiment: scanning electron microscopy (SEM), Raman spectroscopy, and measurements of photoelectric emission yield. A separate section of this chapter is devoted to discussing each technique.

2.1. Scanning Electron Microscopy (SEM)

The Scanning Electron Microscope (SEM) is a microscope that uses electrons rather than light to form an image. There are many advantages to using the SEM instead of a light microscope. The SEM has a large depth of field, which allows a large amount of the sample to be in focus at one time. The SEM also produces images of high resolution, which means that closely spaced features can be examined at a high magnification. Preparation of the samples is relatively easy since most SEMs only require the sample to be conductive. The combination of larger depth of focus, greater resolution,

higher magnification, and ease of sample preparation makes the SEM one of the most heavily used instruments in research areas today [2].

The development of the Scanning Electron Microscope in the early 1950's brought with it new areas of study in the medical and physical sciences because it allowed examination of a great variety of specimens. As in any microscope the main objective is for magnification and focus for clarity. An optical microscope uses lenses to collect the light waves and the lenses are adjusted for focus. In the SEM, electromagnets are used to collect an electron beam, which is used to produce the image on a screen. By using electromagnets an observer can have more control in how much magnification he/she obtains. The electron beam also provides greater clarity in the image produced [2]. Figure 1 shows a picture of the SEM used in this experiment.

Figure 1. A picture of the SEM used in this experiment.

The general operation of an SEM is fairly simple. The SEM uses electrons instead of light to form an image. A beam of electrons is produced at the top of the microscope by heating of a metallic filament. The electron beam follows a vertical path through the column of the microscope. It makes its way through electromagnetic lenses that focus and

direct the beam down towards the sample. Once it hits the sample, other electrons (backscattered or secondary) are ejected from the sample. Detectors collect the secondary or backscattered electrons, and convert them to a signal that is sent to a viewing screen similar to the one in an ordinary television, producing an image [3]. Figure 2 shows a schematic of a SEM [4].

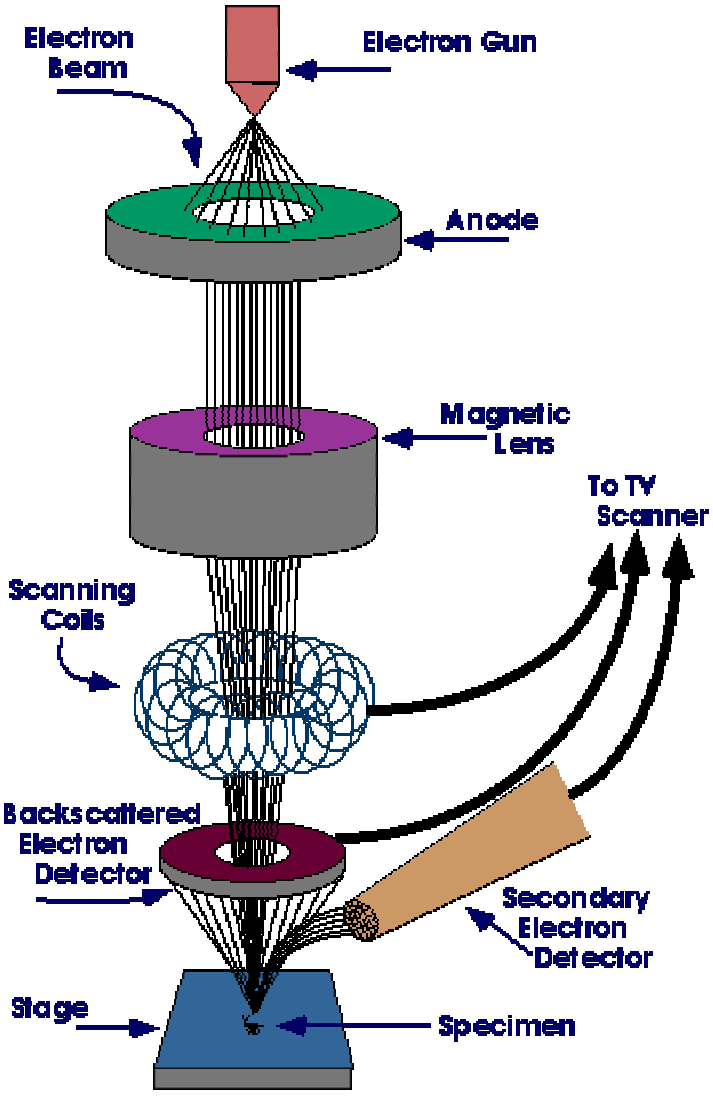

Figure 2. A schematic of a SEM.

The electron beam comes from a filament, that can be made of various types of materials. The most common is the tungsten hairpin gun. This filament is a loop of tungsten that functions as the cathode. A voltage is applied to the loop, causing it to heat up. The anode, which is positive with respect to the filament, forms powerful attractive forces for electrons. This causes electrons to accelerate toward the anode. Some accelerate right by the anode and on down the column, to the sample. Other examples of filaments are lanthanum hexaboride filaments and field emission guns [3]. Figure 3 shows a schematic of the electron gun [4].

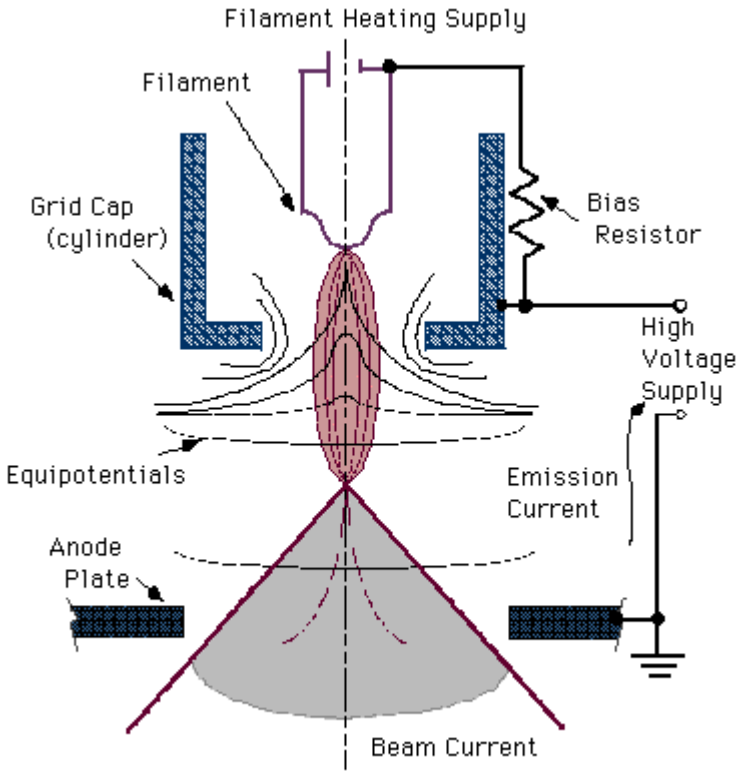

Figure 3. A schematic of the electron gun.

When an SEM is used, the column must always be at vacuum. There are many reasons for this. If the sample is in a gas filled environment, an electron beam cannot be generated or maintained because of a high instability in the beam. Gases could react with the electron source, causing it to burn out, or cause electrons in the beam to ionize, which produces random discharges and leads to instability in the beam. The transmission of the beam through the electron optic column would also be hindered by the presence of other molecules. Those other molecules, which could come from the sample or the microscope itself, could form compounds and condense on the sample. This would lower the contrast and obscure details in the image. A vacuum environment is also necessary for the sample preparation. One such example is the sputter coater, which is a chamber used for coating non-conducting samples with a conducting film. If the chamber is not at vacuum before the sample is coated, gas molecules would get in the way of the argon and gold, two elements used in the coating process. This could lead to uneven coating, or no coating at all [3].

2.2. Raman Spectroscopy

This section discusses the general theory of Raman spectroscopy.

Raman spectroscopy is a very useful technique for characterization of diamond films and has some advantages over other techniques like electron microscopy and electron diffraction [5]. Transmission electron microscopy (TEM), for example, involves a lengthy sample preparation process to allow electron beams to penetrate the diamond films. Moreover, the sample preparation process is destructive. On the other hand, scanning electron beams used in scanning electron microscopy (SEM) deposit electrons

on the diamond film and cause charging problems because diamond films may not be very conducting. Charging hampers the characterization process. Electron diffraction patterns are easily affected by the structure of very small areas of the sample, which can make the results misleading since they would not reflect the overall structure of the sample [6]. In contrast, Raman spectroscopy provides detailed information about the samples to be studied using a relatively easy and non-destructive sample preparation process. The advent of powerful intense monochromatic light sources, such as lasers, and very sensitive photon detectors, such as photomultiplier tubes, made Raman spectroscopy feasible [7].

When a monochromatic beam of radiation of frequency (ω_i) is incident on a sample, a shift occurs in the frequency of the scattered radiation. That is when the scattered radiation is detected not only will (ω_i) be observed, but also ($\omega_s = \omega_i \pm \Delta\omega$). The frequency shift ($\Delta\omega$) is due to the microscopic rotational and vibrational motion of the atoms and molecules in the sample. Such scattering of radiation with frequency shift is termed Raman scattering in honor of the scientist C. V. Raman who was the first to report this phenomenon in 1928 [8].

The frequency shift in Raman scattering is due to the photon-phonon interactions. The photons in the incident beam interact with the quantized vibrations of the lattice in the scattering system. These quantized vibrations are known as phonons. The photon-phonon interactions occur by transfer of energy such that the total energy is conserved. When a photon of energy ($\hbar\omega_i$) is incident on the sample it could trigger a phonon transition from one energy level to the other. One can think of three possible scenarios. The simplest scenario one can think of is when the incident photon passes without

interacting with the lattice, hence the scattered photon has the same energy ($\hbar\omega_i$). The second scenario is when the incident photon triggers a phonon transition from an energy level (E_1) to a higher level (E_2). The upward phonon transition is triggered by the annihilation of the incident photon and the creation of a photon of lower energy, $\hbar$ (ω_i - $\Delta\omega$), and hence of lower frequency. The frequency shift is related to the change in the phonon energy subject to energy conservation as: $\Delta E = E_2 - E_1 = \hbar \Delta\omega$. Conversely, the third scenario occurs when the incident photon triggers a downward phonon transition from (E_2) to (E_1). Now, the outgoing photon has energy, $\hbar$ ($\omega_i + \Delta\omega$), and hence higher frequency. Table 3 summarizes the three scenarios [9].

Table 3. Frequency shift in Raman scattering.

Scenario	Incident Photon Frequency	Phonon Transition	Outgoing Photon Frequency
1	ω_i	None (same E)	ω_i (same frequency)
2 (anti-Stokes)	ω_i	Upward (E_1 to E_2)	$\omega_i - \Delta\omega$ (lower frequency)
3 (Stokes)	ω_i	Downward (E_2 to E_1)	$\omega_i + \Delta\omega$ (higher frequency)

A Raman spectrum is characterized by upward and downward shifts in frequency corresponding to energy gains and energy losses of photons respectively. The energy loss of a photon is called Stokes scattering while the energy gain is called anti-Stokes scattering. The intensity of anti-Stokes to Stokes Raman scattering decays exponentially

as the frequency shift increases since the thermal phonon population of higher energy levels decreases exponentially as the energy difference, ΔE, increases [9].

A Raman spectroscopy system consists of 4 components: a light source, optical setup, a Raman spectrometer, and a photomultiplier tube. The first component of a Raman spectroscopy system is a light source, typically a laser source. An optical setup focuses the beam on the sample of interest. Another optical setup collects the scattered beam and focuses it on the opening of the Raman spectrometer. The Raman spectrometer separates the different frequencies contained in the scattered beam. A photomultiplier tube (PMT) mounted on the exit side of the spectrometer is used to count the number of scattered photons for each frequency. Raman spectrometers now are controlled by a computer that scans the frequency spectrum and captures the Raman spectrum of the sample of interest [9].

The photomultiplier tube is an integral part of a Raman system. The photomultiplier tube is a light detector that is useful in low intensity applications such as fluorescence spectroscopy. Due to high internal gain, photomultiplier tubes are very sensitive detectors. PMTs are similar to phototubes. A photomultiplier tube consists of a photocathode and a series of dynodes in an evacuated glass enclosure. Photons that strike the photoemissive cathode emit electrons due to the photoelectric effect. Instead of collecting these few electrons (there should not be a lot, since the primarily use for PMT is for very low signal) at an anode like in the phototubes, the electrons are accelerated towards a series of additional electrodes called dynodes. These electrodes are each maintained at a more positive potential. Additional electrons are generated at each dynode. This cascading effect creates 10^5 to 10^7 electrons for each photon hitting the first

cathode depending on the number of dynodes and the accelerating voltage. This amplified signal is finally collected at the anode where it can be measured. In other words, a photomultiplier tube converts the incident signal from bursts of photons to voltage pulses which can be counted by a computer [9]. In this experiment, the photomultiplier tube is used to count the number of photons per unit time scattered from the sample after being analyzed by the Raman spectrometer. Figure 4 gives a schematic of PMT [10].

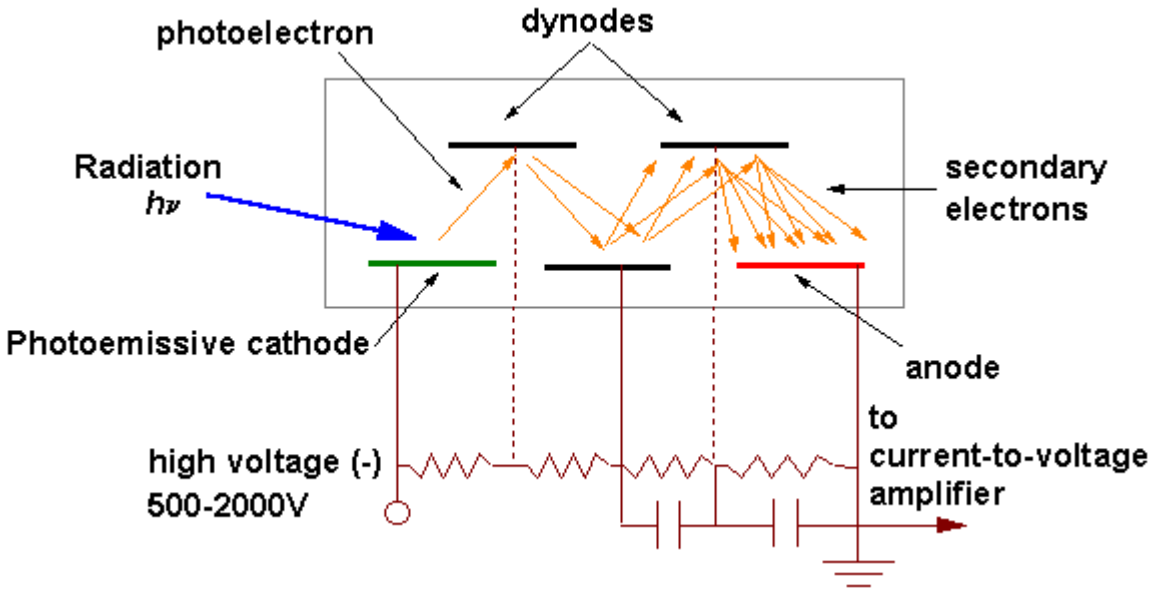

Figure 4. A schematic diagram of a photomultiplier tube.

There are many sources of noise that can affect the performance of a Raman system. The first type of noise is associated with two types of scattering that occur during Raman spectroscopy experiments. One type of scattering occurs due to small scattering centers such as molecules, which is called Rayleigh scattering. Another type results from scattering by large scattering centers such as dust, which is called Mie scattering. These two types always occur during a Raman scattering experiment. The relative intensity of Rayleigh scattering to Raman scattering depends on many factors, such as the physical state of the sample, its chemical composition, and the direction of observation with respect to the direction of the incident beam. Hence, it is difficult to say in general what the relative intensity is expected to be. But one can give a rough estimate and say that the Rayleigh scattering intensity is about 10^{-3} times that of the incident radiation and the Raman scattering intensity is almost 10^{-3} times that of the Raman scattering [11].

Another source of noise is electrical noise from the photomultiplier tube. It is know that any surface whose temperature is above absolute zero emits electrons by thermionic emission. These electrons are registered as counts and are called thermionic dark counts, or simply dark counts, since they occur even in the absence of light [12].

A question that arises while analyzing the data of a Raman scattering experiment is how to improve the signal-to-noise ratio. Let's consider the statistical distribution of pulses coming from background sources. It is modeled as a Poisson distribution. As the number of pulses per second gets large, the distribution converges to a normal one. Therefore, the signal-to-noise ratio in the Raman spectrum is proportional to the square root of the collection time. Hence, it is possible to improve the signal-to-noise ratio by a

factor of two by quadrupling the data collection time or by doubling the power of the incident light [9].

2.3. Microchannel Plate

A microchannel plate was used to do the photoelectric emission measurements. The microchannel plate (MCP) developed as a spin-off of fiber optical technology and is related to the photomultiplier tube and larger single channel conductive glass electron multipliers. They were originally developed for use in night vision systems, but now they are being used in a wide variety of analytical systems such as electron and ion detectors. A microchannel plate is a glass plate with an annular array of thousands of parallel channels, glass tubes10-25 microns in inner diameter and 0.5 to 1 mm long. Each channel acts as a separate electron multiplier. An accelerating potential is applied across the ends of the tubes and when an electron enters the tube it produces additional secondary electrons as a result of striking a special highly emissive coating on the inside of the tube. Thus, after several collisions the original electron may become a thousand or more before exiting the tube. A second tube behind the first further amplifies these emerging electrons creating gains approaching 10^7. The front surface of the detector array may be biased positively or negatively to attract or repel secondary electrons from the sample. In this way a secondary image or backscattered image may be easily selected. Figure 5 shows a schematic of a microchannel plate [13].

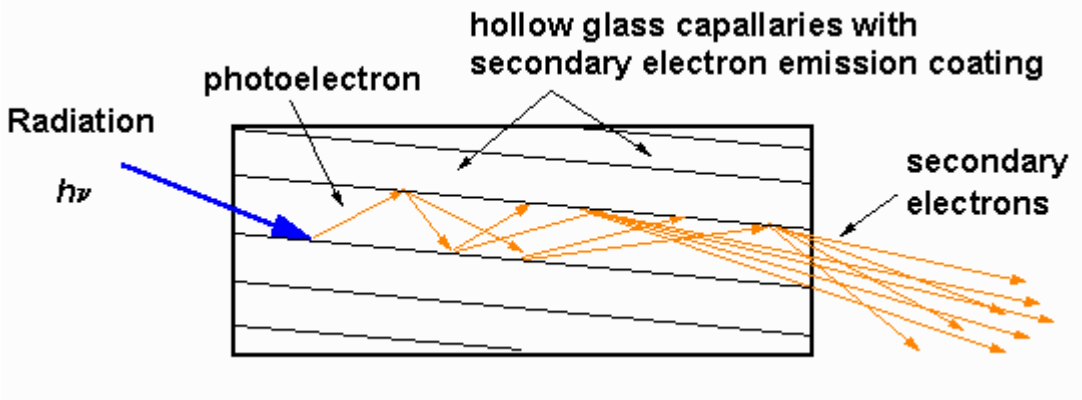

Figure 5. A schematic diagram of a microchannel plate.

2.4. Experimental Setup

This section discusses the experimental setup used in this experiment for Raman spectroscopy and photoelectric emission measurements. The setup allows for the simultaneous measurement of Raman spectroscopy and photoelectric emission. Figure 6 shows a schematic of the setup.

The light source used is a Coherent Innova 90 Argon ion laser having a maximum power of 5 Watts for all lines in the spectra. The laser produces 8 lines in the visible region ranging from 4579 A to 5145 A. Table 4 lists the wavelengths and energies for the laser lines. It is necessary to use visible light to be able to excite electrons from unoccupied states, as will be further discussed in chapter 3.

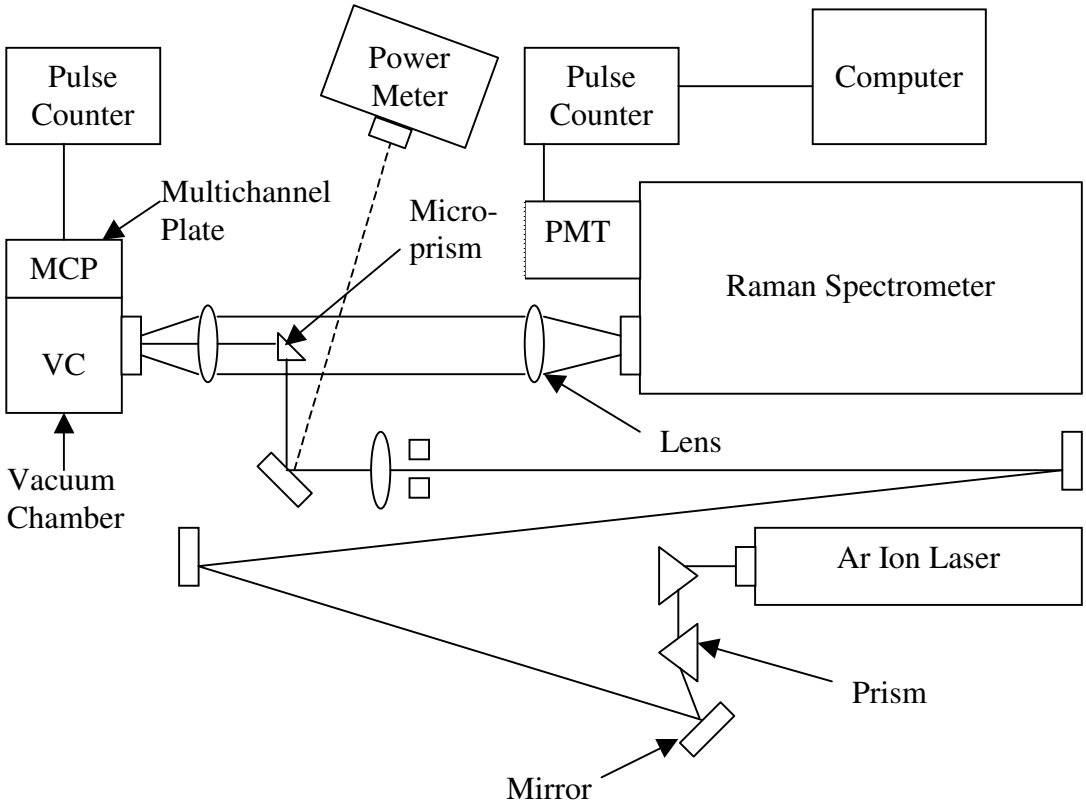

Figure 6. The experimental setup for Raman and photoelectric measurements.

Table 4. Laser lines used in this experiment.

Wavelength (A)	Energy (eV)
5145	2.410
5017	2.472
4965	2.497
4880	2.541
4765	2.602
4727	2.623
4658	2.662
4579	2.7080

Ultraviolet lines of wavelengths 3511 A and 3638 A can be obtained using special optics [14]. Plasma lines are removed from the laser beam by using two prisms in front of the laser and also a long optical path. The laser beam is deflected towards the sample, as shown in figure 6, using a very small prism which does not obstruct the path of the laser beam scattered from the sample to the spectrometer. Then the laser beam is focused on the opening of the vacuum chamber containing the diamond samples using a lens.

Six diamond samples have been studied having different methane concentrations ranging from 0.2% to 1.6%. The sample was housed in a vacuum chamber having a pressure of $6x10^{-9}$ torr. The samples were lined up vertically inside the chamber and the sample that the laser beam was aimed at was selected using a linear translator built in the chamber.

A BrightView model XUV-2018 microchannel plate is connected to the vacuum chamber to measure the photoelctron emission rate from the sample of interest due to the incident laser beam. The emission rate is measured using a pulse counter attached to the multichannel plate.

The laser beam scattered from the sample is collected using a lens right in front of the opening of the vacuum chamber. The laser beam is then focused on the opening of the Raman spectrometer using another lens. A Spex 1404 0.85 mm double spectrometer was used. A Hamamatsu 943 photomultiplier tube was attached to the spectrometer to detect the number of photons per unit time for each laser wavelength scattered from the sample after being analyzed by the Raman spectrometer. The photomutliplier tube was connected to a pulse counter which was then attached to a computer which captures the Raman spectrum. A power meter was also used for measuring the power of the incident laser beam. This was accomplished by deflecting the laser beam towards the power meter, bypassing the sample.

Six polycrystalline CVD diamond film samples have been studied. The methane concentrations used during the growth process relative to hydrogen are: 0.10%, 0.30%, 0.45%, 0.60%, 0.70%, and 0.80%. A list of the growth parameters is as follows:

- Temperature: 900°C
- Tungsten filament temperature: 2200°C
- Pressure: 30 torr
- Growth time: 2 hours
- Hydrogen flow rate: 200 SCCM
- Film thickness: 2 microns

- Substrate used: Si pretreated by scratching with diamond powder
- Post growth treatment: none

CHAPTER 3

RESULTS AND DISCUSSION

This chapter discusses the results obtained in this experiment and the interpretations of these results. Similar to chapter two, it is divided into four sections: the first one discusses the SEM micrographs obtained for the samples, the second discusses the Raman spectra, the third discusses the photoelectric emission yield results, and the last section discusses the interpretations of all of these results.

3.1. SEM Results

The scanning electron microscope (SEM) is a very useful tool for determining the morphology of diamond films. The general operation of SEM was discussed in section 2.1. This section discusses SEM micrographs obtained for the samples under study.

Many properties of a material are determined by its structure. Diamond has a unique crystal structure that leads to a unique combination of properties. Diamond has a faced-centered cubic (fcc) space lattice as shown in figure 7. The diamond structure has a characteristic tetrahedral bonding. Each atom has 4 nearest neighbors and 12 next nearest neighbors. The diamond structure is relatively empty; the maximum proportion of the

available volume that may be filled by hard spheres is only 0.43, which is 46% of the filling factor for a closest-packed structure such as fcc or hexagonal closed packed (hcp). The diamond structure is an example of the directional covalent bonding found in column IV of the periodic table of elements. Not only carbon, but also silicon, germanium, and tin can crystallize in the diamond structure [15].

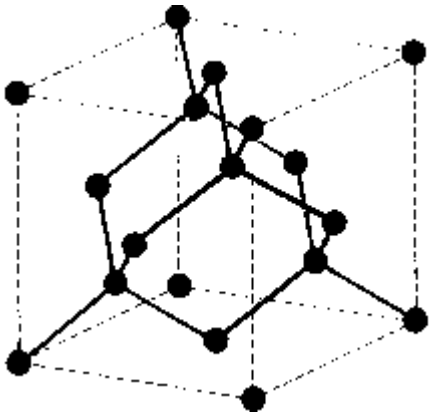

Figure 7. Crystal structure of diamond, showing the tetrahedral bond arrangement.

By comparing the SEM micrographs presented in this section for diamond samples with different methane concentrations, one can study how the morphology of the sample depends on the methane concentration used in the growth process. The higher the methane concentration the higher the defect density, and hence the lower the quality of the diamond. Moreover, as the methane concentration increases the sample becomes predominantly amorphous. The bar mark on each micrograph specifies the scale in microns. The first set of micrographs, figure 8, refers to a diamond sample with 0.45% methane concentration. These micrographs show that the sample is predominantly

crystalline and that the diamond crystals in the sample are of high quality. On the other hand, figures 9 and 10 refer to two samples having higher methane

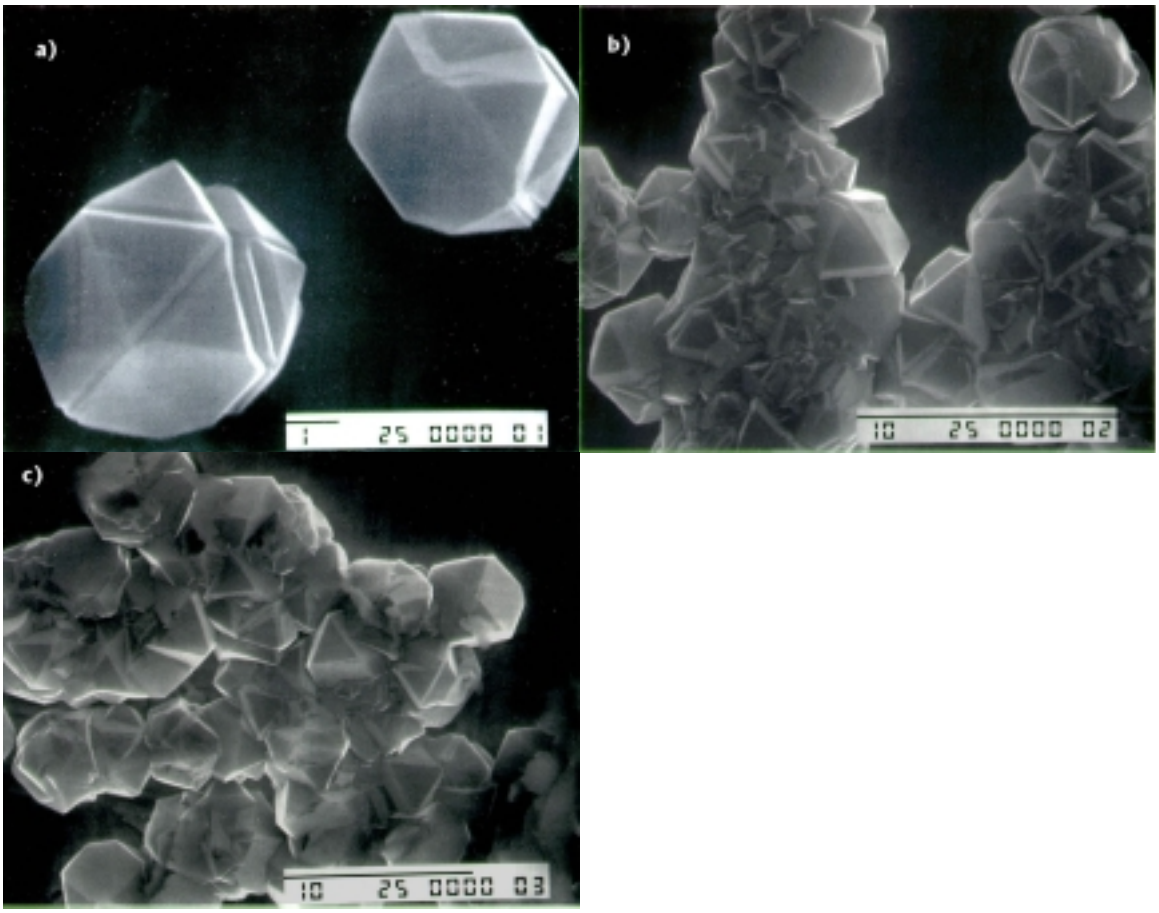

Figure 8. SEM micrographs for a high quality CVD polycrystalline diamond film with 0.45% methane concentration. a) Two high quality twin diamond crystals. The triangular faces are (111) planes. The square ones are (100) planes. b) A region of high quality diamond crystals closely packed. c) The same region at lower magnification. This diamond sample is of high quality because of the relatively low methane concentration, which leads to low defect density.

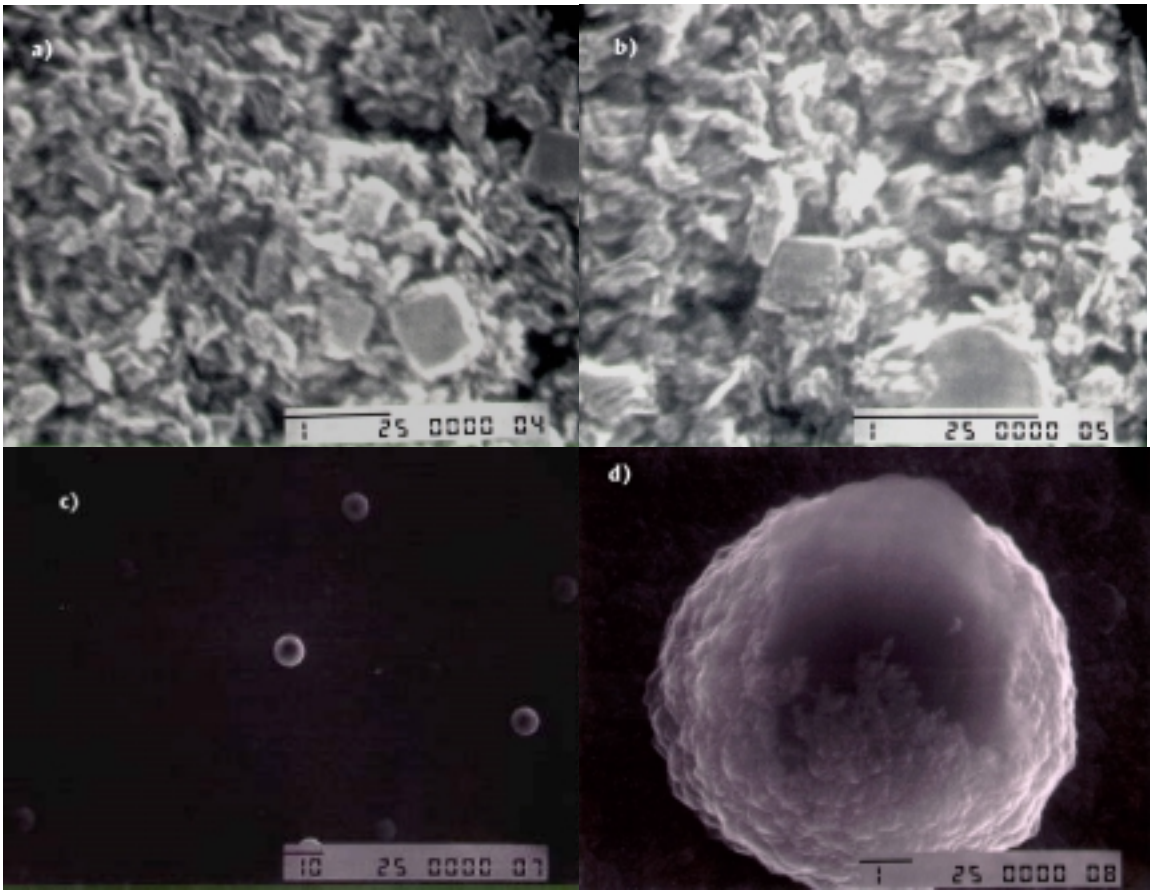

Figure 9. SEM micrographs for a low quality CVD polycrystalline diamond film with 0.80% methane concentration. a) Low quality diamond crystals closely packed in a region of the sample. b) The same region at higher magnification. c) A different region of the sample with islands of amorphous carbon. d) A zoomed-in image of an amorphous carbon island. This diamond sample is of low quality because of the relatively high methane concentration, which leads to high defect density.

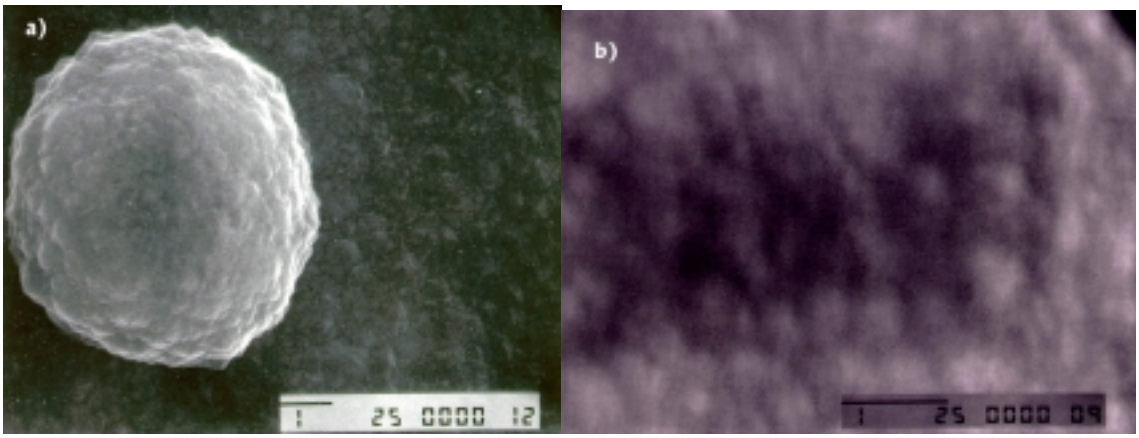

Figure 10. SEM micrographs for a low quality CVD polycrystalline diamond film with 0.70% methane concentration. a) A region of amorphous carbon. b) A zoomed-in picture of the same region. The morphology of this sample is, as expected, very similar to that of the previous one since the difference in methane concentration is very small.

concentrations; 0.70% and 0.80% respectively. These samples are predominantly amorphous and the diamond crystals contained in the samples are of low quality. The change of composition with the change in methane concentration is treated quantitatively in section 3.2 on Raman spectra.

3.2. Raman Spectra

Raman spectroscopy is a very useful tool for determining the composition of CVD diamond films. By knowing the composition of each sample one can reason about the defect density in that specific sample. To determine the composition the Raman spectrum needs to be fitted to a statistical distribution. In this experiment, the fitting is done using the software Peakfit [16] and the Lorentzian distribution is used. The software decomposes the Raman spectrum into a number of peaks, each corresponding to a component of the sample. The Raman spectra for two of the samples are fitted. Then, the Raman spectra for all the samples are presented.

Figures 11 and 12 show the curve fitting for the samples with 0.10% and 0.60% methane concentration respectively. Tables 5 and 6 list the peaks existing in each spectrum. Each spectrum has 4 peaks. Figures 13 through 18 show the Raman spectra for all six samples studied. The clear difference in the overall shape from one spectrum to the other is due to the difference in composition. However, it is very difficult to get any quantitative information about the composition of each sample just by inspecting the spectrum. For this purpose one has to curve-fit the spectrum.

By inspection of figures 11 and 12 and tables 5 and 6 one can notice the change in composition of the samples as the methane concentration used during growth changes.

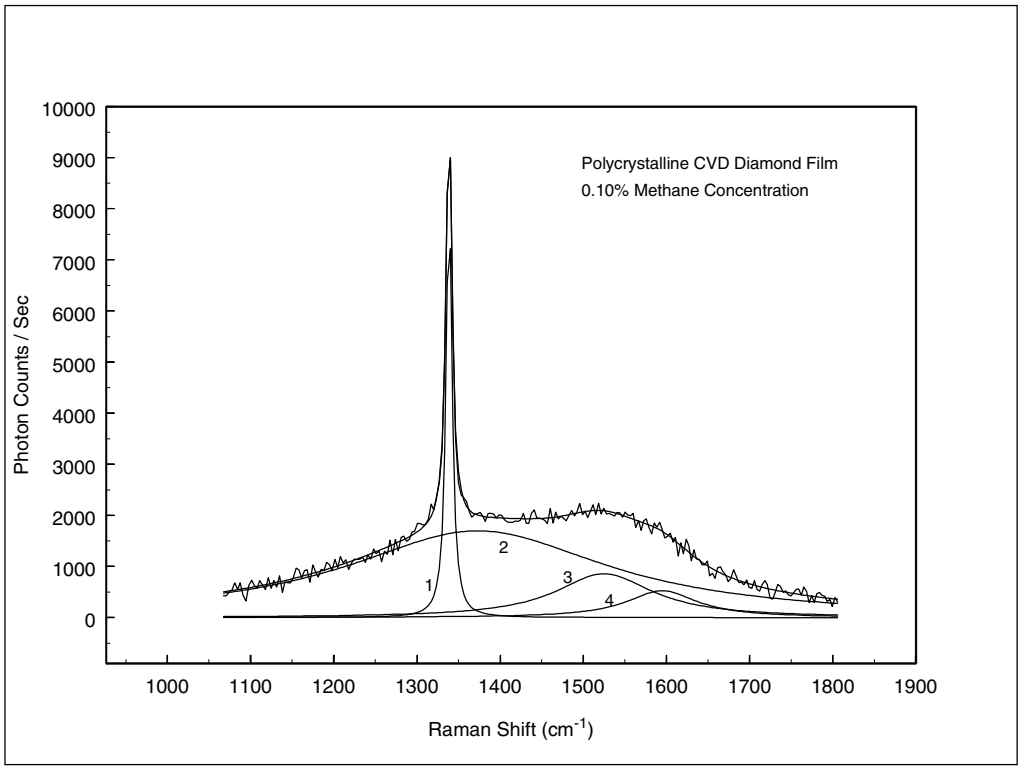

Figure 11. Raman spectrum and peaks for CVD polycrystalline diamond with 0.1% methane concentration.

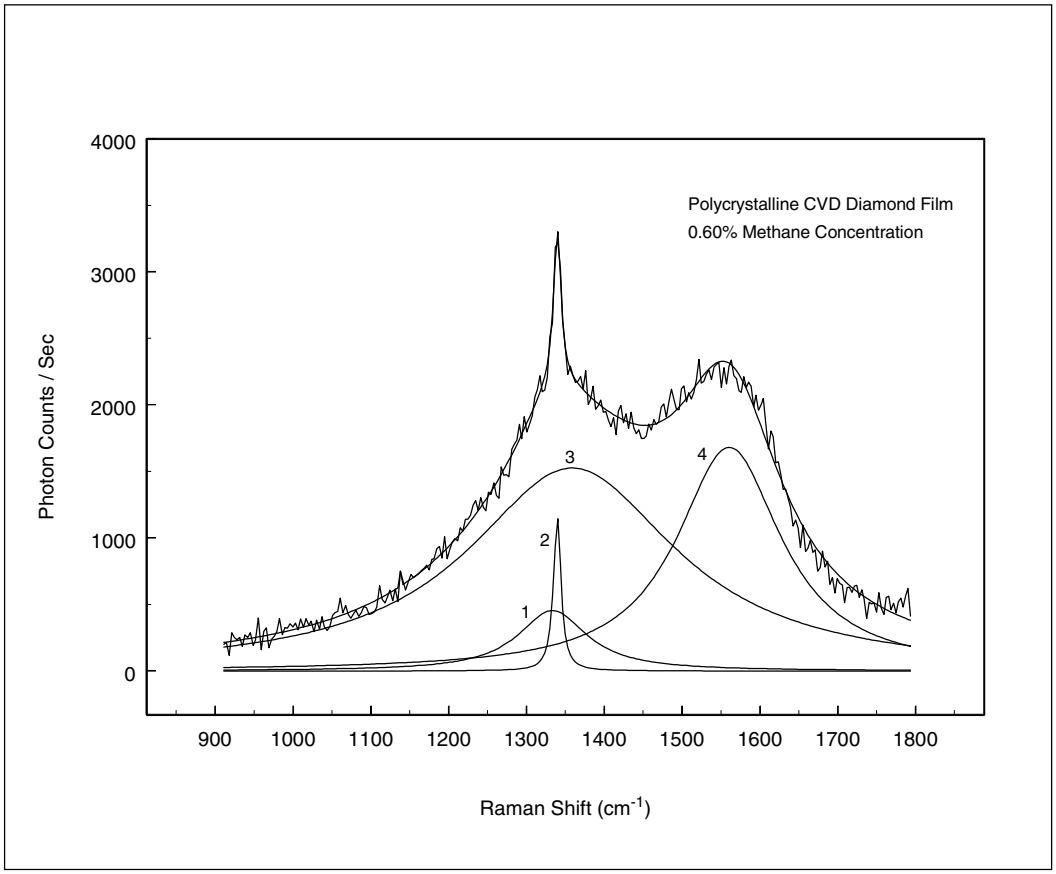

Figure 12. Raman spectrum and peaks for CVD polycrystalline diamond with 0.6% methane concentration.

Table 5. Raman peaks for a CVD polycrystalline diamond film with 0.10% methane concentration.

Peak No.	Center (cm^{-1})	Percentage Area (%)	Amplitude (Photons/Sec)	FWHM (cm^{-1})	Component
1	1339	10.2	7878	4	Crystalline diamond
2	1373	66.7	1698	191	Nanocrystalline graphite
3	1525	15.9	859	71	Amorphous sp^2-sp^3
4	1595	7.2	525	52	Crystalline graphite

Table 6. Raman peaks for a CVD polycrystalline diamond film with 0.60% methane concentration.

Peak No.	Center (cm^{-1})	Percentage Area (%)	Amplitude (Photons/Sec)	FWHM (cm^{-1})	Component
1	1333	6.7	454	54	Nanocrystalline graphite
2	1340	1.9	1153	6	Crystalline diamond
3	1359	56.9	1526	164	Amorphous sp^2-sp^3
4	1560	34.5	1682	82	Crystalline graphite

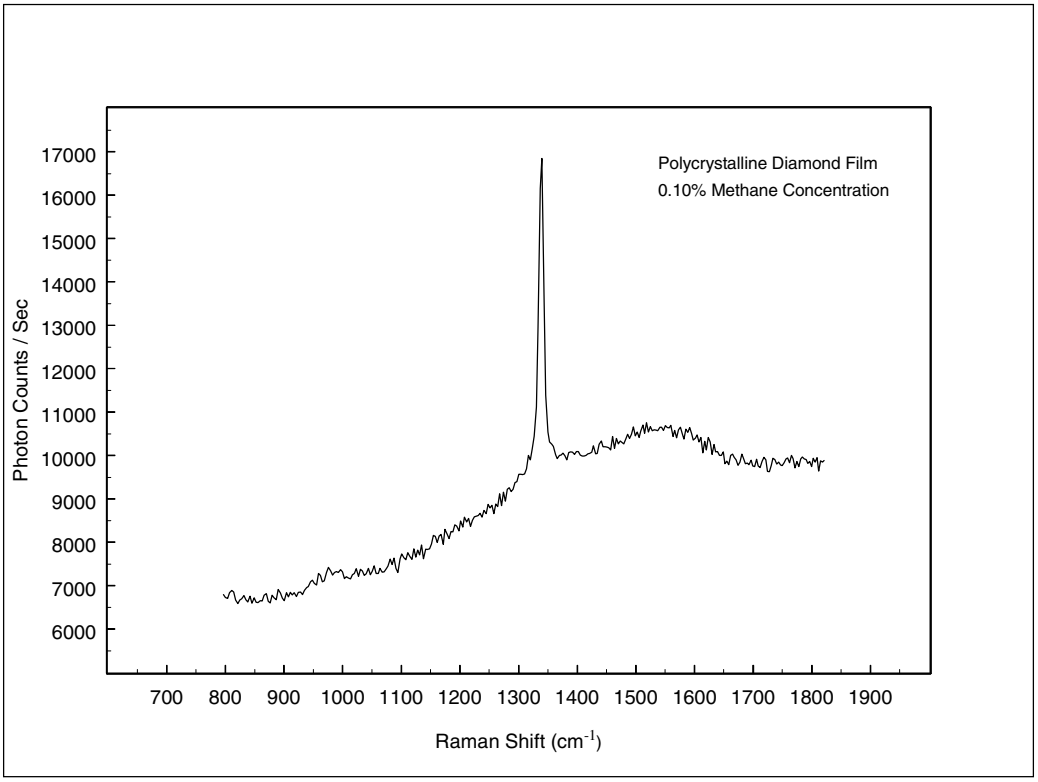

Figure 13. Raman spectrum for a polycrystalline CVD diamond film with a 0.10% methane concentration.

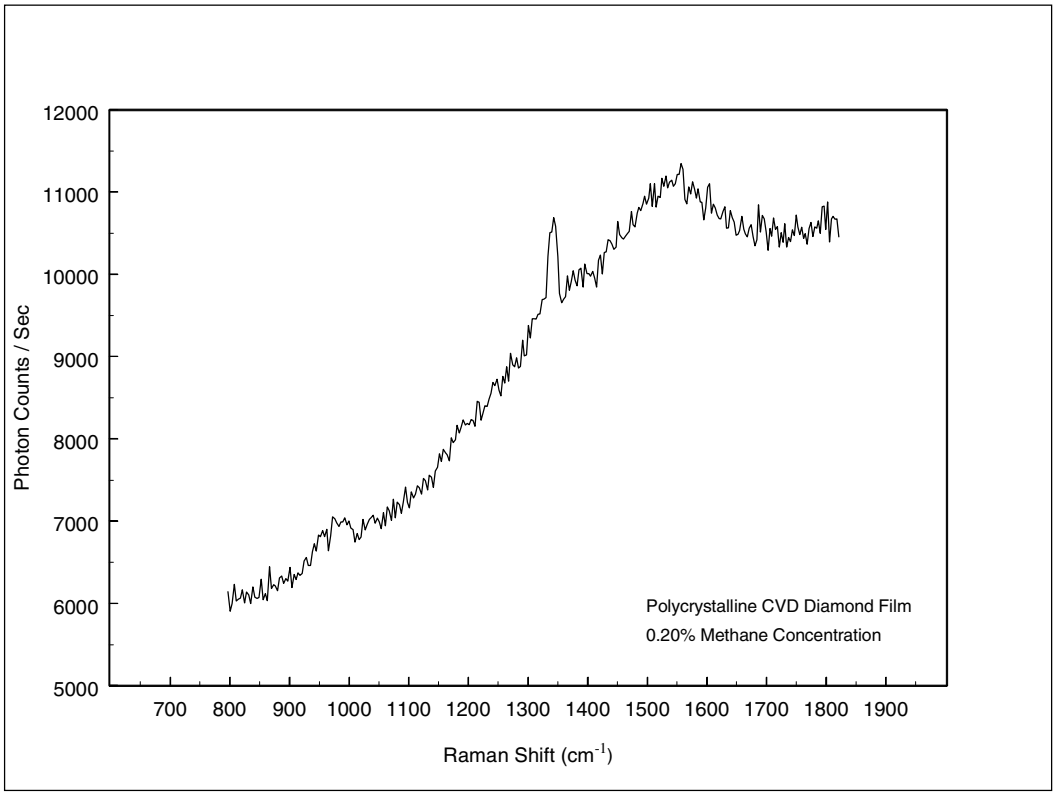

Figure 14. Raman spectrum for a polycrystalline CVD diamond film with a 0.30% methane concentration.

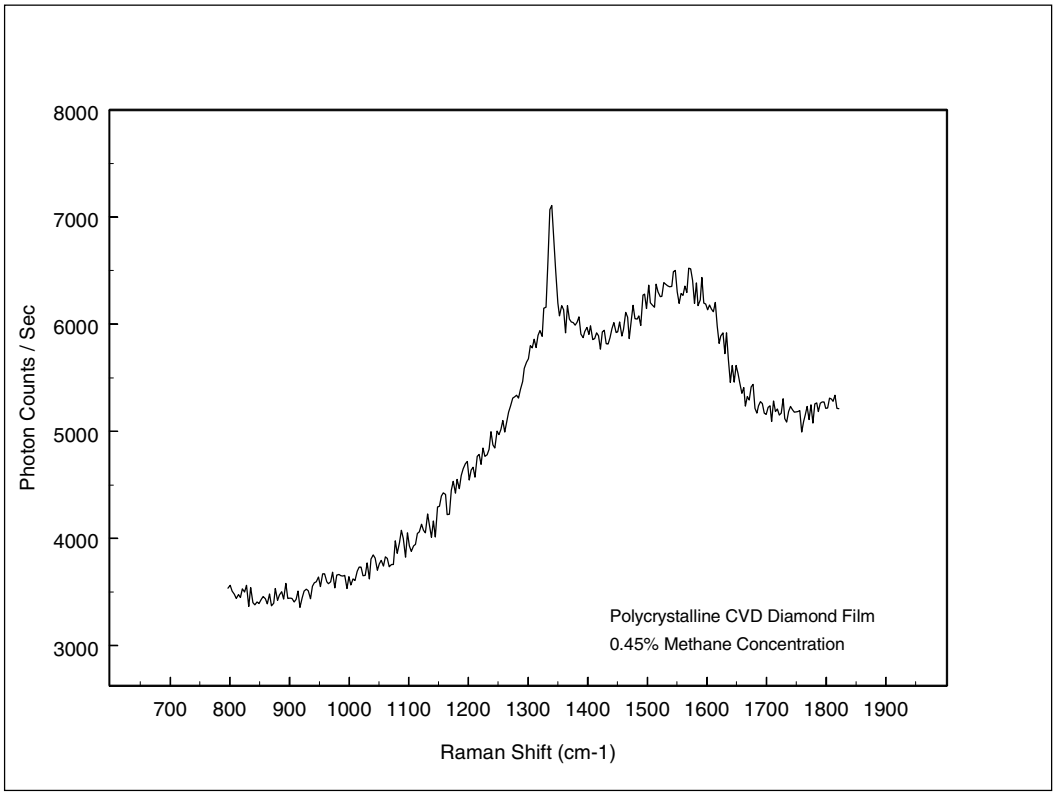

Figure 15. Raman spectrum for a polycrystalline CVD diamond film with a 0.45% methane concentration.

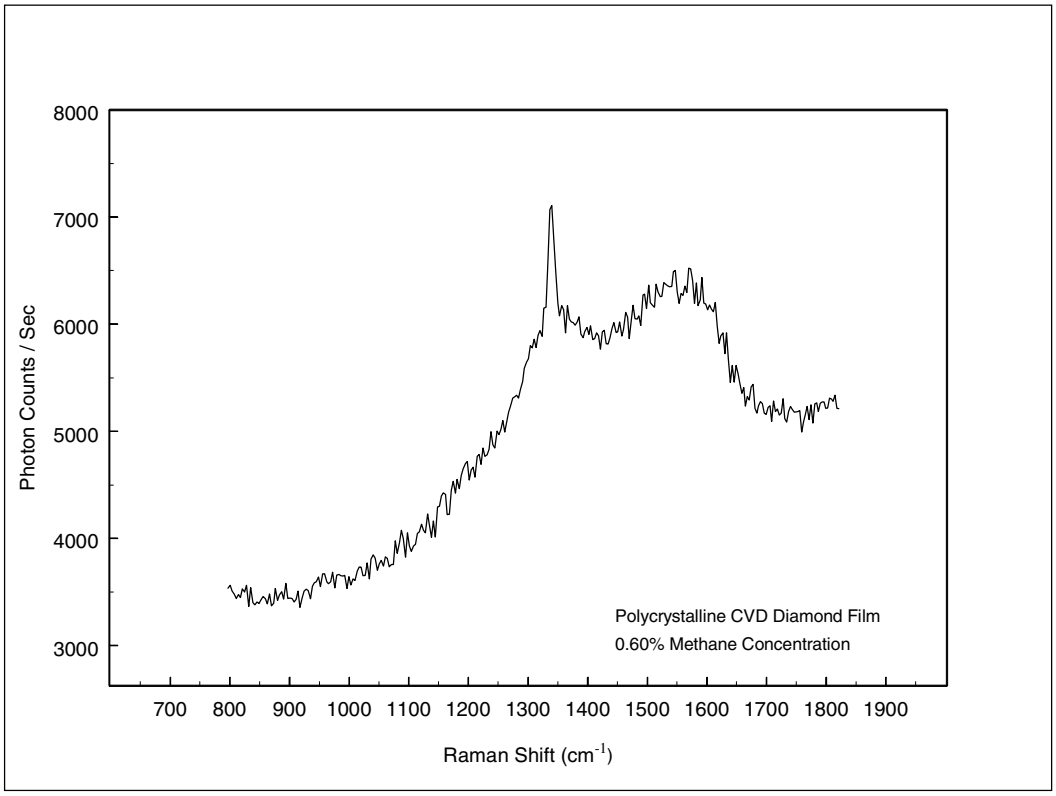

Figure 16. Raman spectrum for a polycrystalline CVD diamond film with a 0.60% methane concentration.

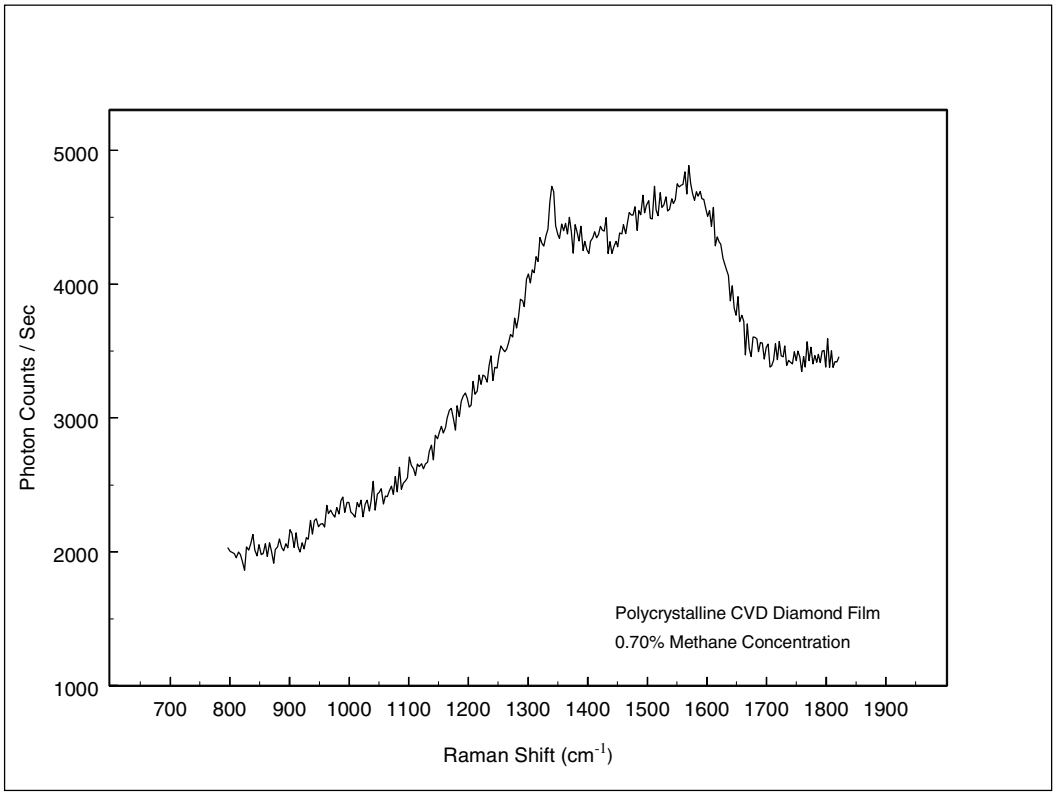

Figure 17. Raman spectrum for a polycrystalline CVD diamond film with a 0.70% methane concentration.

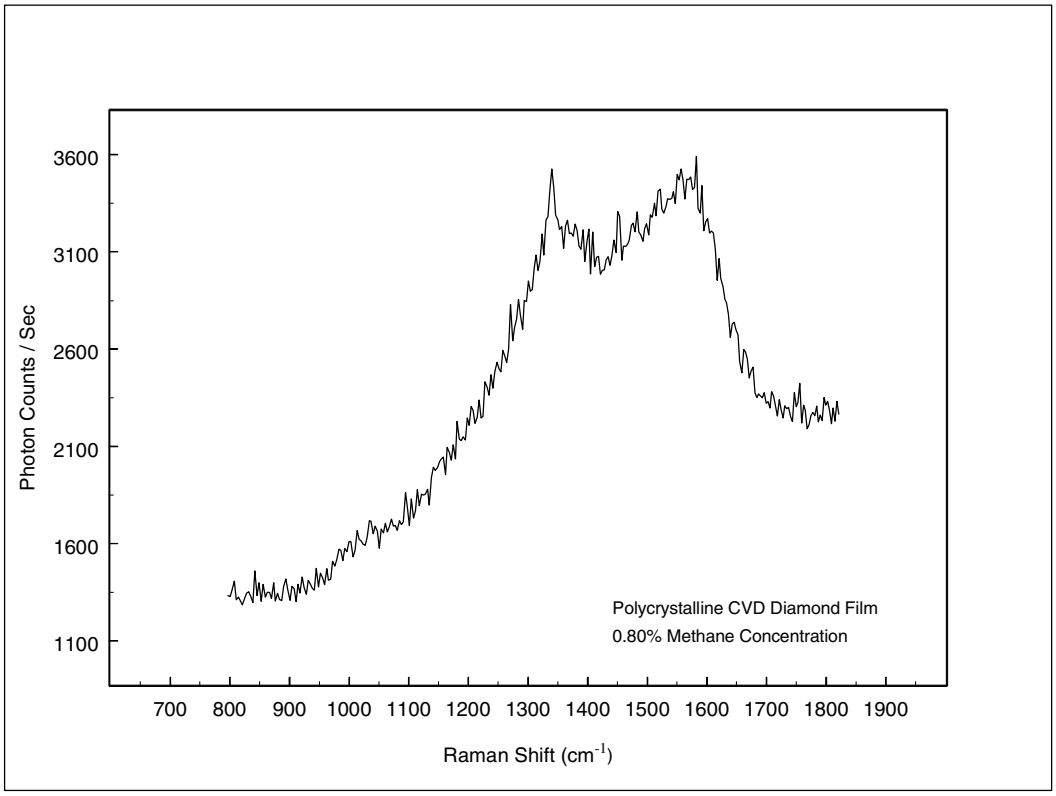

Figure 18. Raman spectrum for a polycrystalline CVD diamond film with a 0.80% methane concentration.

The sample presented in figure 12 corresponds to a much higher methane concentration compared to that of figure 11: 0.60% as opposed to 0.10% respectively. Correspondingly, the percentage of crystalline diamond compared to other components in the sample in figure 12 is much lower than that in figure 11: 1.9% as opposed to 10.2%. Moreover, the percentage of amorphous sp^2-sp^3 in the sample in figure 12 is much higher than that in figure 11: 56.9% as opposed to 15.9%. Furthermore, the full width at half maximum (FWHM) of the diamond peak in figure 12 is slightly larger than that in figure 11, implying lower quality diamond in figure 12 compared to figure 11. However, the slight change in FWHM might be due to noise and could depend on the fitting parameters. This comparison leads to the conclusion that the sample in figure 12 has a higher defect density than that in figure 11, since defects are more likely to exist in amorphous regions. The same conclusions were drawn in a qualitative way in the previous section, section 3.1, on SEM micrographs.

3.3. Photoelectric Yield Results

This section discusses the photoelectric emission results for the diamond samples studied in this experiment. First, the photoelectric emission rate as a function of laser beam power is curve-fitted. Then, the photoelectric yield as a function of energy is plotted for each sample to show the dependence of the photoelectric yield on the methane concentration. These results help understand the photon process underlying photoelectric emission and how it depends on the defect density.

Four different models are used for curve-fitting the photoelectric emission rate. The curve-fitting was done using a data analysis software called Axum 5.0. Follows a list of the models and the name used to refer to each model throughout this document:

- Linear: $y(x) = ax$
- Quad1: $y(x) = ax^2$
- Quad2: $y(x) = ax^2 + bx$
- Quad3: $y(x) = ax^2 + bx + c$

In all the plots, the continuous line refers to the actual data and the dashed one refers to the fitting curve. The signal-to-noise ratios for the last three samples are too low to make any conclusions about the model to be used in fitting the data. However, the plots for the quad1 model for these samples are included for comparison.

The photon process underlying photoelectric emission from the diamond samples studied in this experiment can be understood by comparing the plots presented in figures 19 through 33. The best fit can be determined by inspection of the plots for the different models and also using the standard deviation of error. The standard deviation of error for the linear model is relatively large. Hence, the data cannot be modeled linearly. The standard deviation of error for the quad3 model is small enough. However, the corresponding fitting curves are physically inconsistent. The photoelectric emission rate should be zero at zero power, which is not true the quad3 model. Therefore, the quad3 model has to be excluded. This leaves us with the quad1 and quad2 models; both have very small standard deviation of error and are physically consistent. Therefore, each is a very good candidate for a fitting model. The fitting parameter (b) in the formula for the quad2 model is very small compared to the parameter (a). In other words, for our

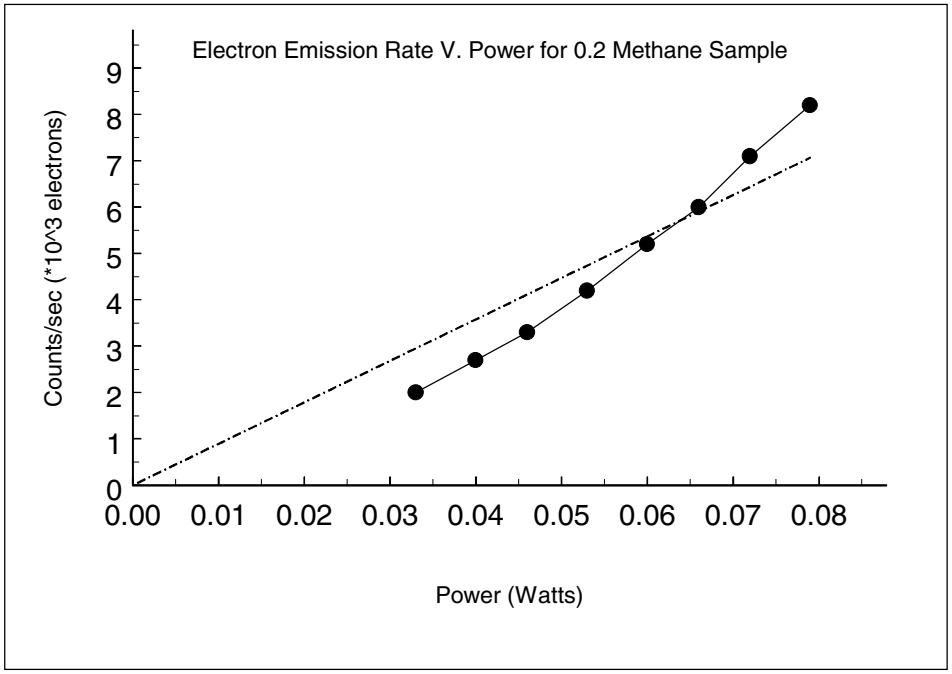

Figure 19. Photoelectric emission rate v. laser power for a polycrystalline CVD diamond film with a 0.10% methane concentration. Linear - standard deviation = 0.79.

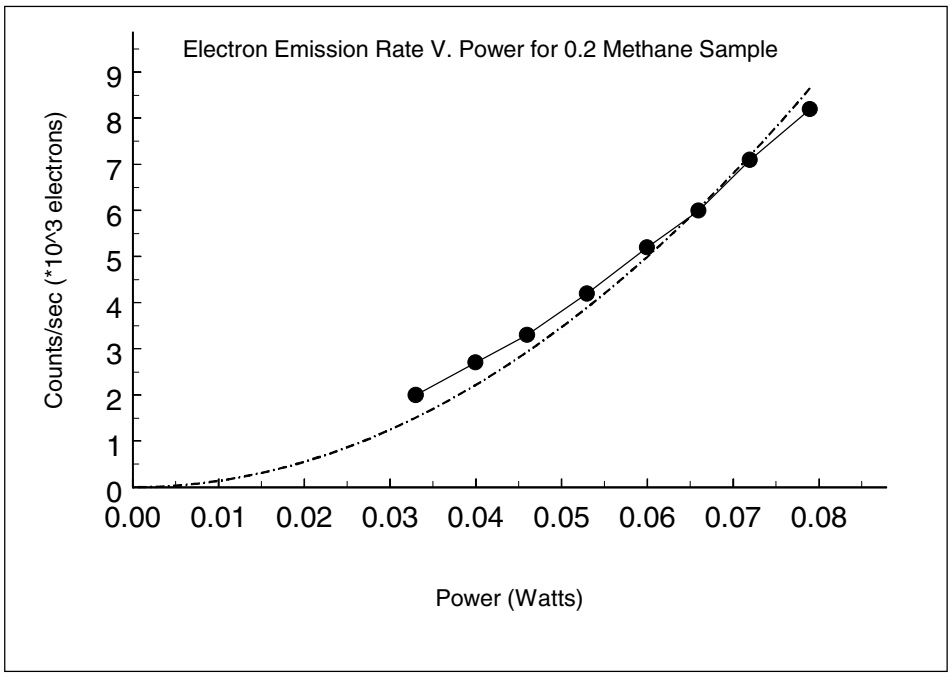

Figure 20. Photoelectric emission rate v. laser power for a polycrystalline CVD diamond film with a 0.10% methane concentration. Quad1 - standard deviation = 0.37.

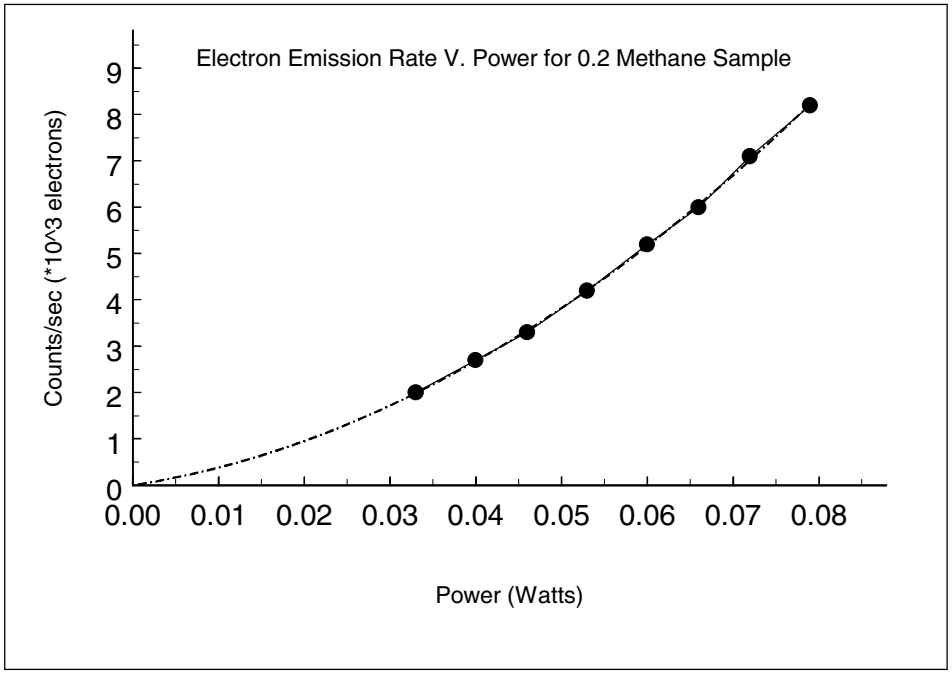

Figure 21. Photoelectric emission rate v. laser power for a polycrystalline CVD diamond film with a 0.10% methane concentration. Quad2 - standard deviation = 0.05.

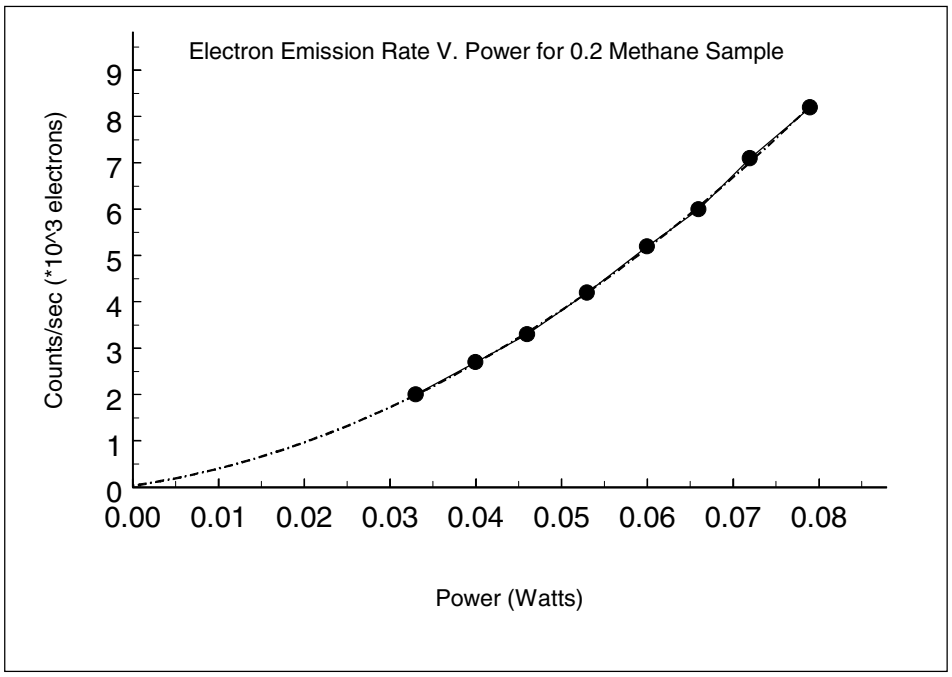

Figure 22. Photoelectric emission rate v. laser power for a polycrystalline CVD diamond film with a 0.10% methane concentration. Quad3 - standard deviation = 0.05.

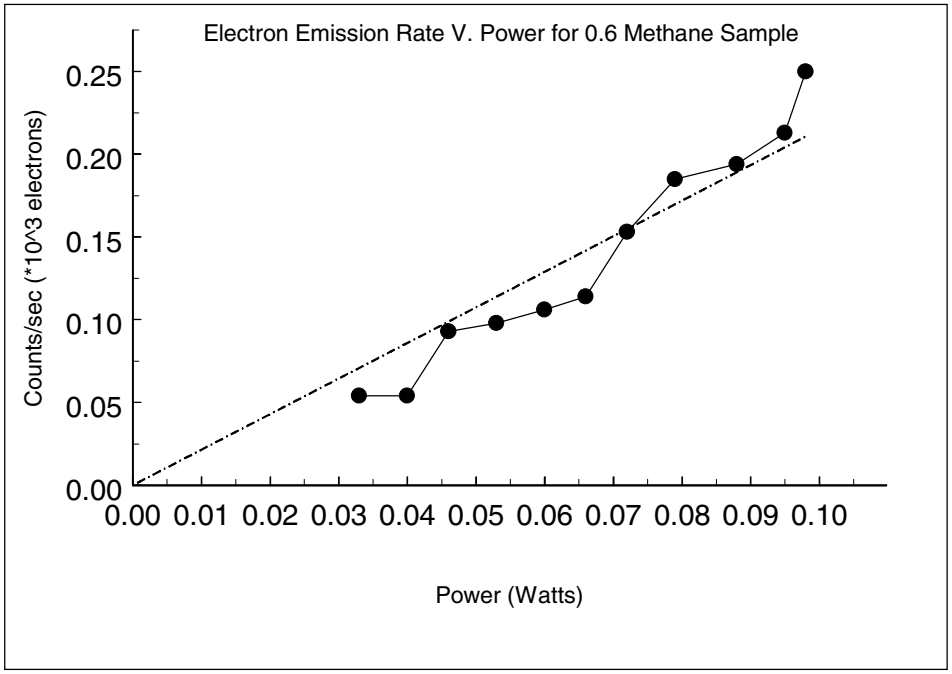

Figure 23. Photoelectric emission rate v. laser power for a polycrystalline CVD diamond film with a 0.30% methane concentration. Linear - standard deviation = 0.02.

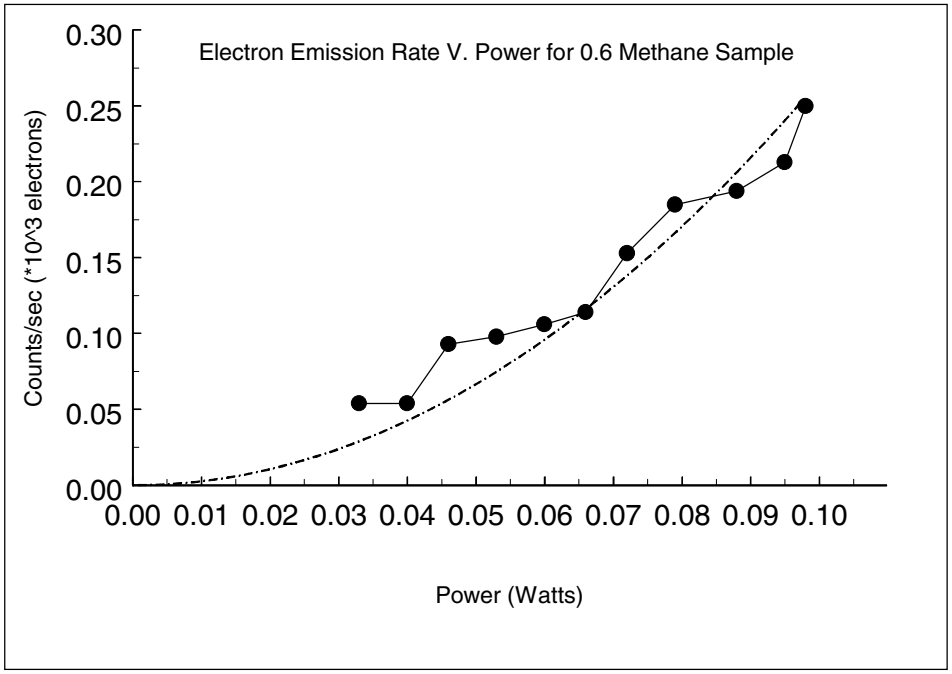

Figure 24. Photoelectric emission rate v. laser power for a polycrystalline CVD diamond film with a 0.30% methane concentration. Quad1 - standard deviation = 0.02.

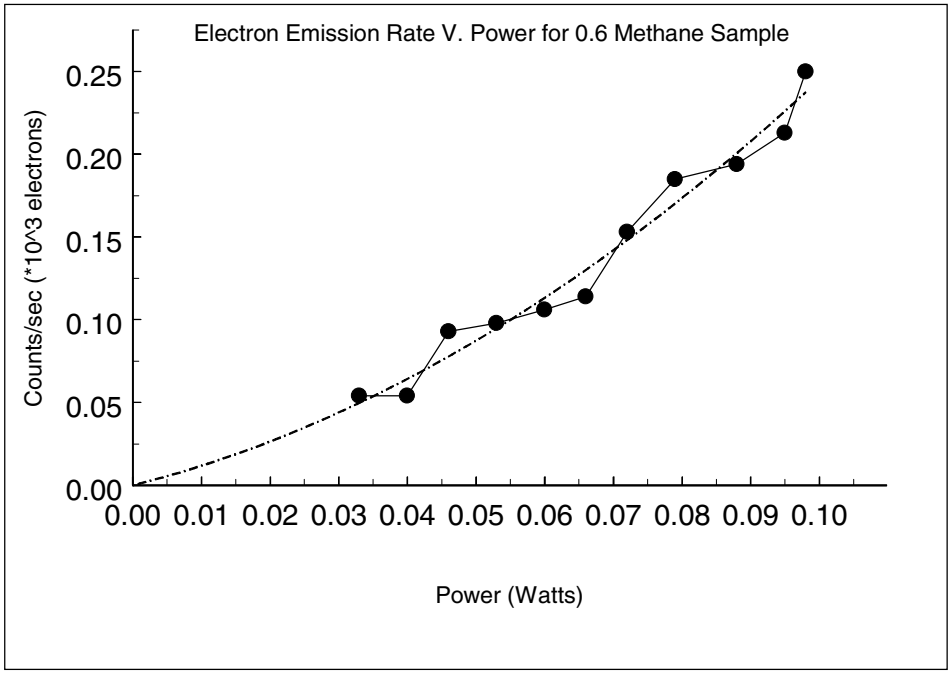

Figure 25. Photoelectric emission rate v. laser power for a polycrystalline CVD diamond film with a 0.30% methane concentration. Quad2 - standard deviation = 0.01.

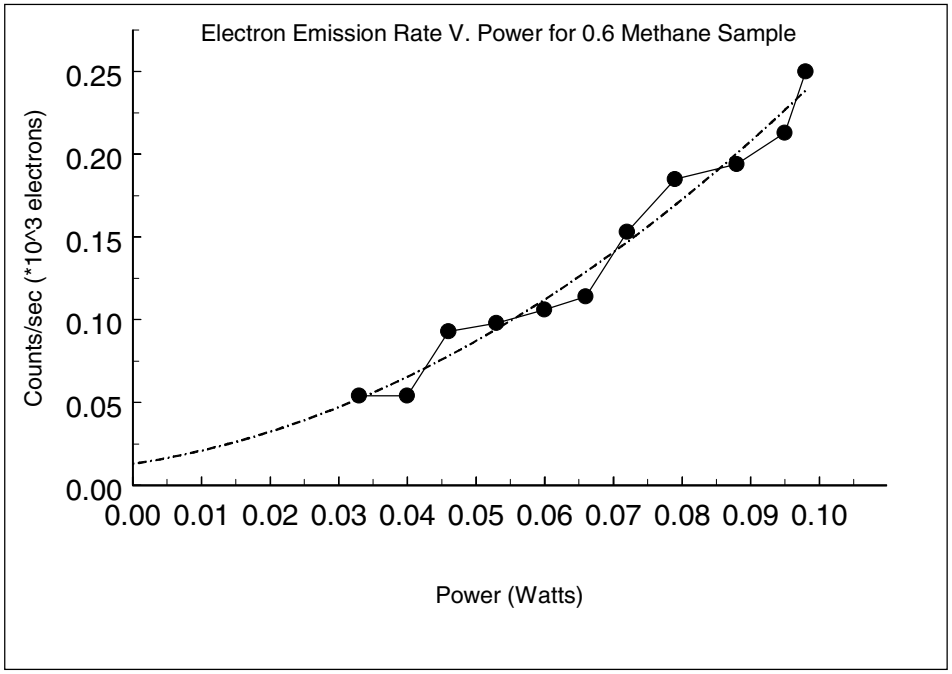

Figure 26. Photoelectric emission rate v. laser power for a polycrystalline CVD diamond film with a 0.30% methane concentration. Quad3 - standard deviation = 0.01.

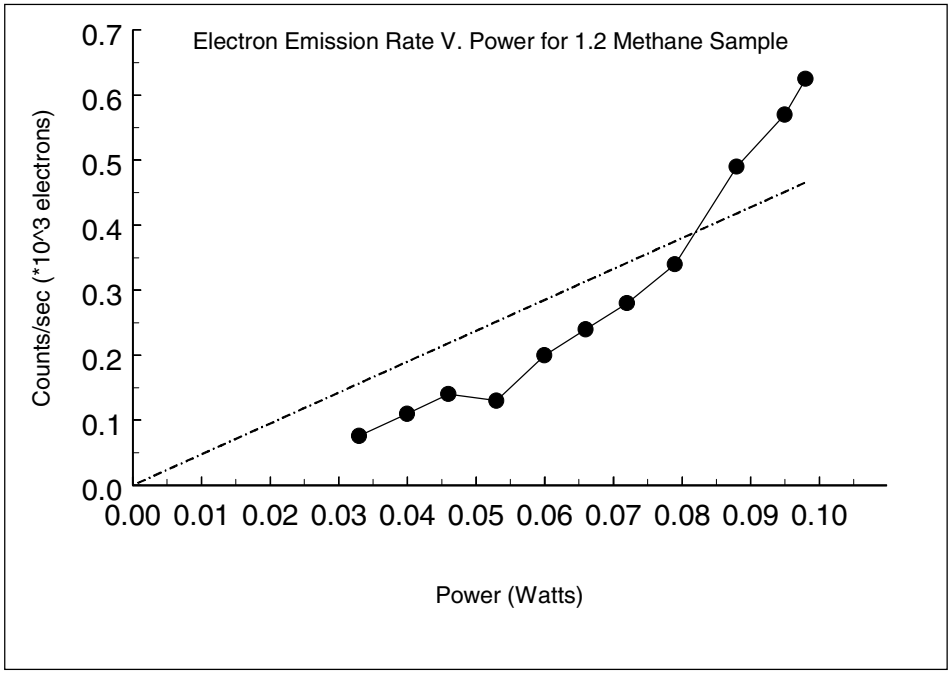

Figure 27. Photoelectric emission rate v. laser power for a polycrystalline CVD diamond film with a 0.60% methane concentration. Linear - standard deviation = 0.10.

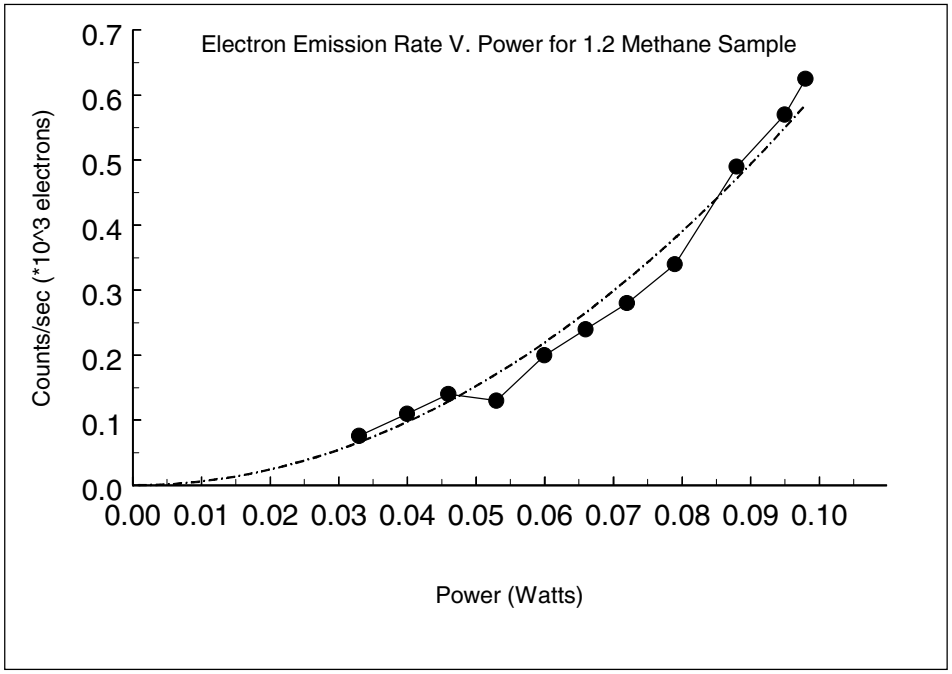

Figure 28. Photoelectric emission rate v. laser power for a polycrystalline CVD diamond film with a 0.60% methane concentration. Quad1 - standard deviation = 0.03.

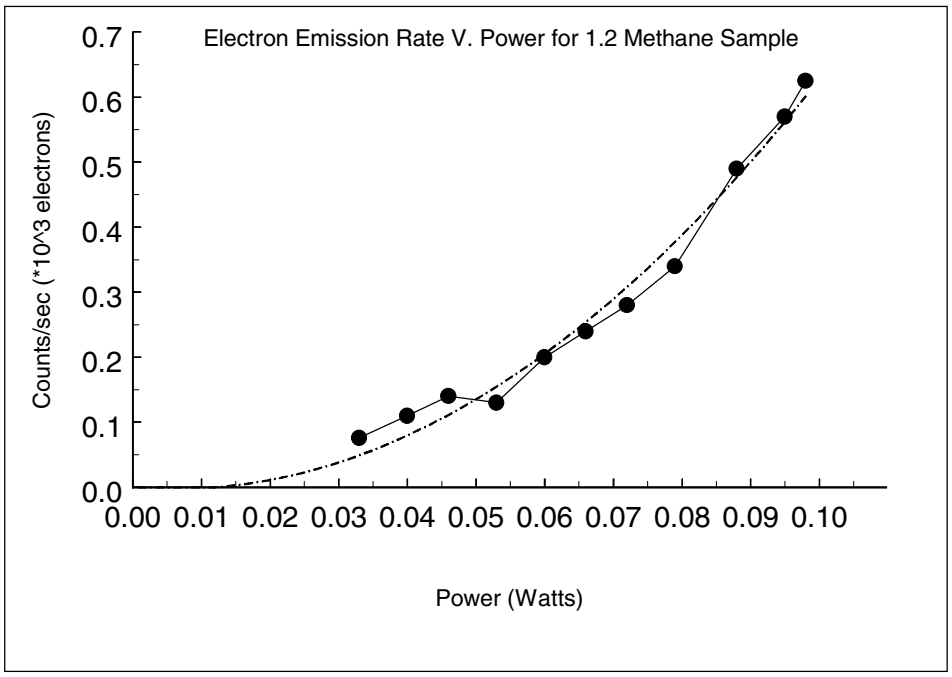

Figure 29. Photoelectric emission rate v. laser power for a polycrystalline CVD diamond film with a 0.60% methane concentration. Quad2 - standard deviation = 0.03.

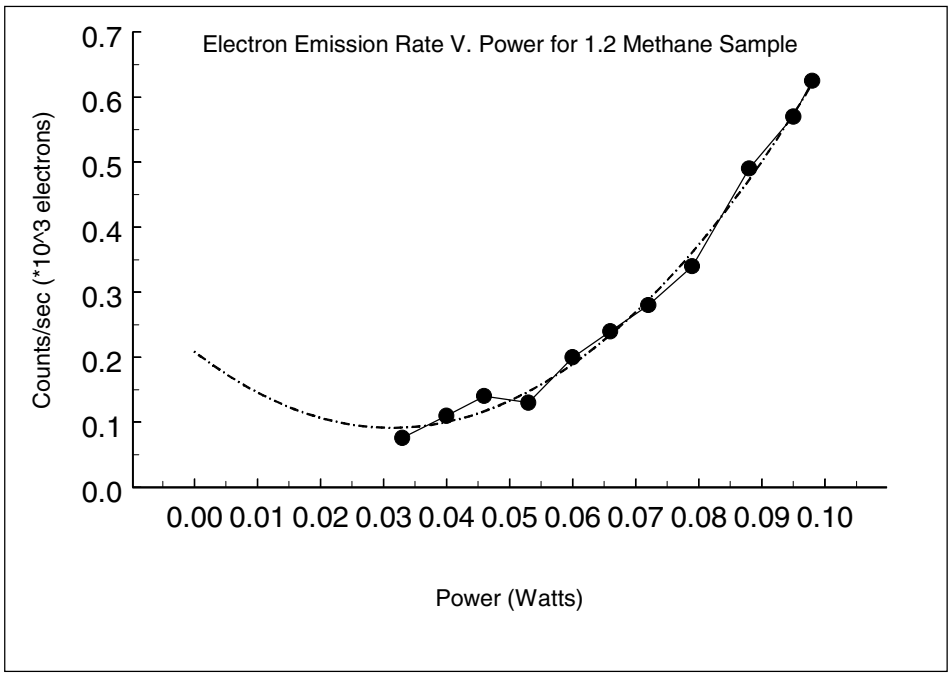

Figure 30. Photoelectric emission rate v. laser power for a polycrystalline CVD diamond film with a 0.60% methane concentration. Quad3 - standard deviation = 0.02.

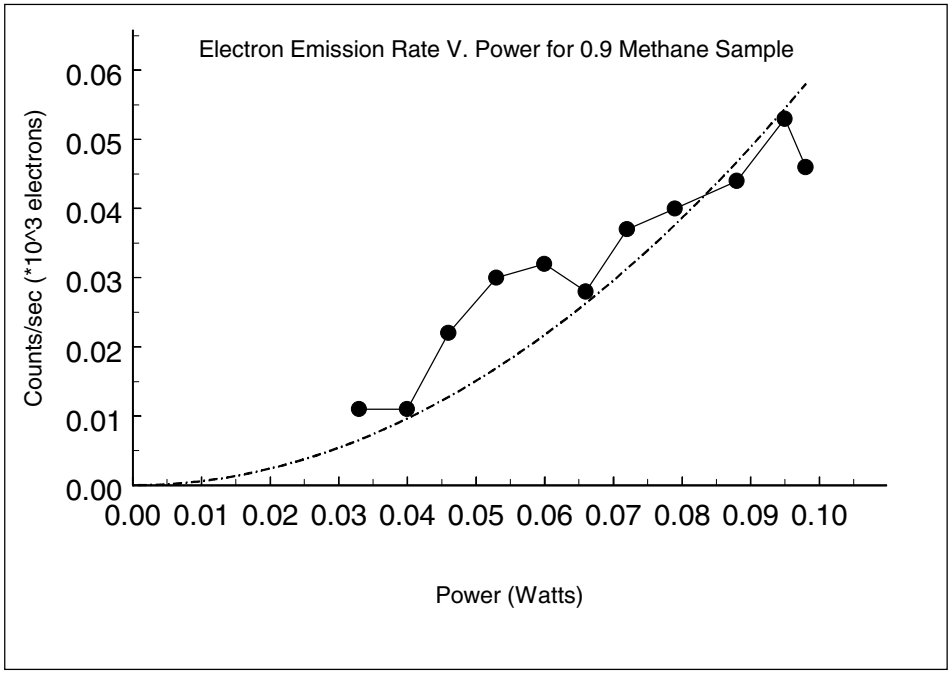

Figure 31. Photoelectric emission rate v. laser power for a polycrystalline CVD diamond film with a 0.45% methane concentration. Quad1 - standard deviation = 0.01.

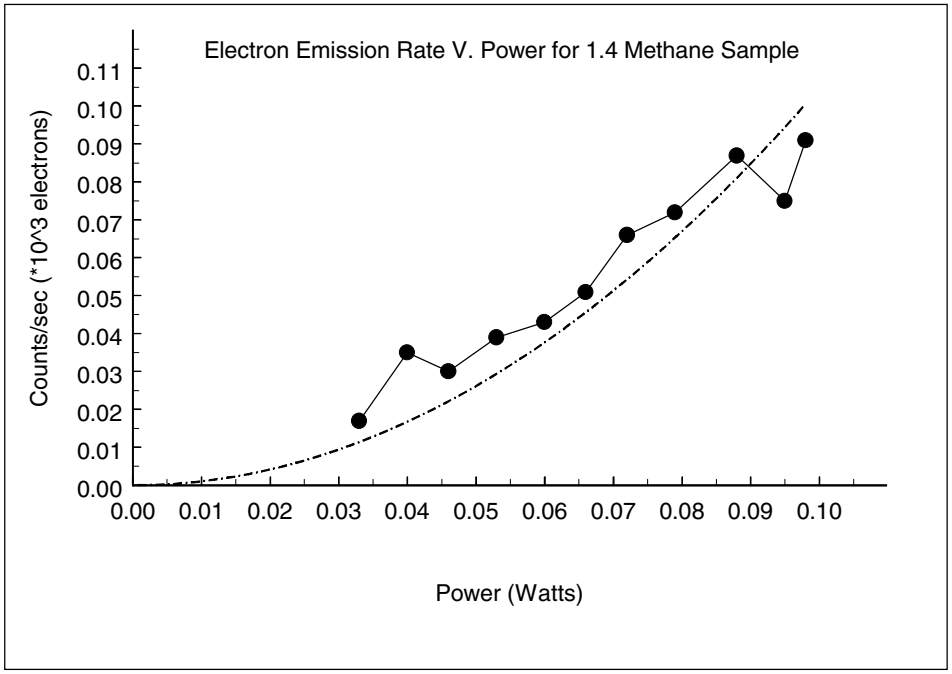

Figure 32. Photoelectric emission rate v. laser power for a polycrystalline CVD diamond film with a 0.70% methane concentration. Quad1 - standard deviation = 0.01.

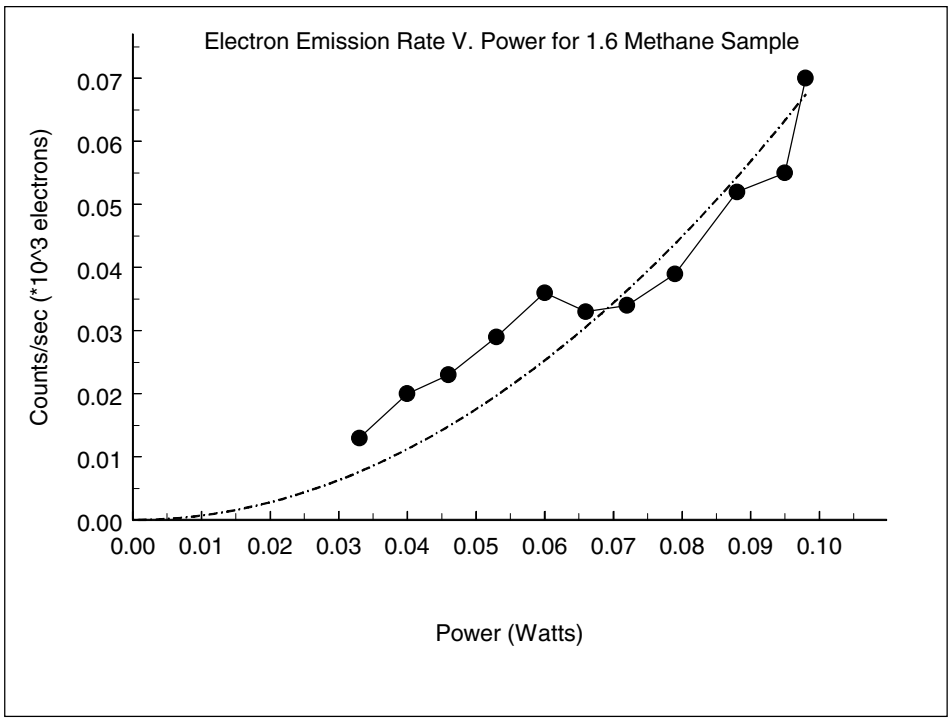

Figure 33. Photoelectric emission rate v. laser power for a polycrystalline CVD diamond film with a 0.80% methane concentration. Quad1 - standard deviation = 0.01.

purposes, the quad2 model reduces to quad1. This leads to the conclusion that photoelectric emission from CVD polycrystalline diamond films is a two-photon process. One-photon processes occur in one step: the excitation of an electron from an initial state to the vacuum occurs through one transition. Therefore, one-photon electron emission processes have a linear dependence between the photoelectric yield and the incident light power. On the other hand, for an electron to undergo a two-photon process the excitation from the initial state to the vacuum occurs through two transitions, passing by an intermediate normally unoccupied state. This results in a quadratic relationship between photoelectric emission yield and incident light power. For example, if one doubles the incident light power, the number of normally unoccupied states filled with electrons doubles. Twice as many of these filled normally unoccupied states are then subsequently excited resulting in four times the resulting emission rate [17,18].

Studying the dependence of the photoelectric yield on the incident photon energy for samples with different methane concentrations helps understand the dependence of the photoelectric yield on the defect density in the samples. The photoelectric yield is defined as the number of electrons emitted from the sample due to one incident photon. The photoelectric yield is calculated by dividing the photoelectric emission rate by the rate at which the photons are incident on the sample. The photoelectric emission rate is measured experimentally using a microchannel plate. The photon incidence rate is calculated by dividing the laser power by the photon energy.

$$\eta = \frac{R}{P/h\nu}$$

The symbols are defined as follows:

η: is the photoelectric yield (dimensionless),

R: is the photoelectric emission rate in counts/sec,

P: is the laser power, and

ν: is the laser frequency.

Figure 34 shows the plots of photoelectric yield v. incident photon energy for samples with different methane concentrations. The methane concentration relative to hydrogen is shown as a percentage next to each plot. It was shown in the first part of this section that each of these plots can be modeled as a two-photon process. Furthermore, figure 34 shows that the photoelectric yield, for the samples under study, decreases with the increase in methane concentration used during the growth process.

3.4. Data Interpretation

Based on the SEM and Raman results discussed in sections 3.1 and 3.2 one can conclude that the graphitic and amorphous carbon content of diamond films increases with the increase in methane concentration. This implies that the defect density in diamond samples increases with the increase in methane concentration since defects are most likely to be found in the graphitic and amorphous regions. Moreover, the data of section 3.3 show that photoelectric emission from diamond is a two-photon process,

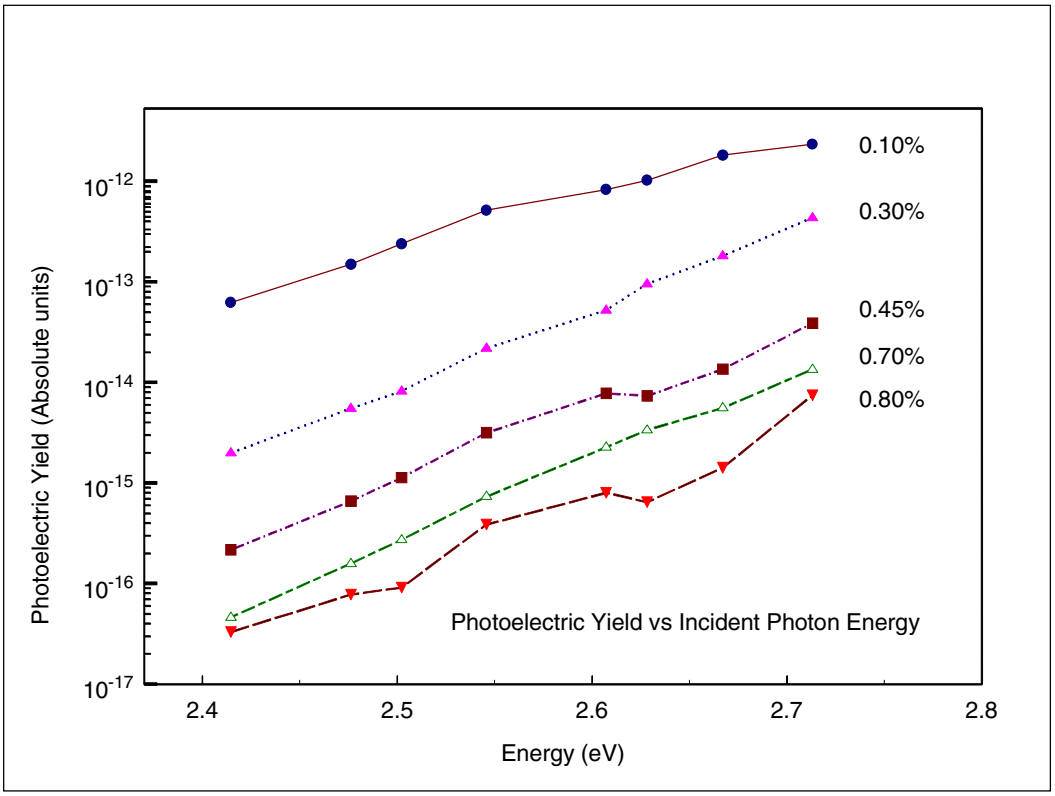

Figure 34. Photoelectric yield v. incident photon energy for samples with different methane concentrations. The methane concentration relative to hydrogen is shown as a percentage next to each plot.

which means that the electrons are emitted from normally unoccupied states. It has been reported in the literature that field emission from diamond increases with the increase in methane concentration. To investigate this issue we studied the photoelectric emission yield versus photon energy for different methane concentrations. The photoelectric yield results presented in section 3.3 show that the photoelectric yield decreases with the increase in methane concentration. This can be interpreted in two different ways. One way is to conclude that the number of unoccupied defects decreases as the methane concentration increases. Since field emission is known to increase as the methane concentration increases [19,20,21], this implies that the unoccupied defects do not participate in field emission. An alternative explanation would be to argue that the defects observed in this experiment do contribute to field emission, but as the methane concentration changes another factor also changes, namely the negative electron affinity (NEA) of diamond.

Negative electron affinity is a phenomenon observed in diamond according to which the vacuum level is below the top of the conduction band. In a typical intrinsic semiconductor the energy difference between the vacuum level and the top of the conduction band is called the electron affinity, χ. When the vacuum level, E_{vac}, is located above the top of the conduction band, E_c, the electron affinity is positive. The positive electron affinity presents an energy barrier for electrons leaving the surface of a material. The work function, Φ, of an intrinsic semiconductor is defined as the energy difference between the Fermi level, E_F, and the vacuum level, E_{vac}. For an intrinsic semiconductor, the Fermi level is located in the middle of the band gab, E_g, which is the energy

difference between the bottom of the conduction band, E_c, and the top of the valence band, E_v. The threshold energy for electron emission, E_T, is given by: $E_T = \chi + E_g$.

For a negative electron affinity surface, the vacuum level is located below the bottom of the conduction band. Therefore, the electron affinity is negative. Negative electron affinity does not mean a zero or negative work function because the vacuum level is still located above the Fermi level. However, on an NEA surface, electrons that arrive at the conduction band can readily escape into vacuum because there is no energy barrier. Therefore, photoelectric emission can take place with photo-excitation at the band gap energy. It is reported that CVD diamond films show NEA [22].

Therefore, one way to account for the photoelectric emission results obtained in this experiment is to argue that the number of normally unoccupied defects remains the same or increases as the methane concentration increases. However, the increase in methane concentration leads to an increase in the electron affinity of the surface which reduces the overall photoelectric yield, counterbalancing the increase in photoelectric yield that would have been produced by the increase in defect density.

CHAPTER 4

CONCLUSIONS

We examined CVD grown polycrystalline diamond films having different methane concentrations to detect defects and study the possible correlation between the methane concentration used during the growth process and the defect density. SEM and Raman results show that as the methane concentration increases the amorphous and graphitic content of the samples increases and the diamond crystal quality diminishes. Therefore, the defect density increases with the increase in methane concentration, which agrees with the results found in the literature. Furthermore, the measurements of the photoelectric emission rate as a function of incident photon energy for different methane concentrations show that photoelectric emission from diamond is due to a two-photon process which means that the electrons are emitted from normally unoccupied states. It is reported in the literature that the field emission from diamond increases with the increase in methane concentration due to the increase in defect density. But we noticed that the photoelectric yield, for our samples, decreases with the increase in methane concentration. This trend can be accounted for in two different ways. One can argue that the defects detected in this experiment decrease in density as the methane concentration increases and, hence, do not contribute to field emission. Consequently, this brings up the

question, currently being debated, of whether and to what extent defects contribute to field emission from diamond. A different approach to account for these results is to argue that the defects we observe indeed contribute to field emission. However, the increase in methane concentration leads to an increase in NEA, which reduces the overall photoelectric yield even though the defect density may increase.

To decide on one of the two scenarios it is necessary to do further experimentation using higher energy photons, for example, from a Xenon lamp in combination with a monochromator leading to a photon energy of ~ 5 eV. In this way, the electrons excited into the conduction band would have enough energy to overcome the electron affinity barrier, and hence the electron affinity, in case it changes, would not affect the photoelectric yield results. If the photoelectric yield still decreases with the increase in methane concentration, then one can conclude that the defects detected in this experiment decrease in density as the methane concentration increases and, consequently, do not play a role in field emission. Consequently, one can conclude that not all defects play a role in field emission. Otherwise, if the trend reverses and the photoelectric yield increases with the increase in methane concentration, then the trend reported in this experiment would be due to an increase in the electron affinity.

REFERENCES

1. K. E. Spear and J. P. Dismukes, *Synthetic Diamond: Emerging CVD Science and Technology* (John Wiley & Sons, New York, 1994).

2. L. F. Stanley, J. W. Heckman, Jr., and K. L. Klomparens, *Scanning and Transmission Electron Microscopy: an Introduction* (W.H. Freeman, New York, 1993).

3. R. E. Lee, *Scanning Electron Microscopy and X-Ray Microanalysis* (Prentice Hall, Englewood Cliffs, 1993).

4. surf.eng.iastate.edu

5. M. N. Yoder, in *Diamond and Diamond-like Films and Coatings*, edited by R. E. Clausing, L. L. Horton, J. C. Angus, and P. Koidl (Plenum Press, New York, 1991).

6. K. H. Chen, Y. L. Lai, L. C. Chen, J. Y. Wu, and F. J. Kao, *Thin Solid Film,* **270**, 143 (1995).

7. W. A. Yarbrough and R. Messier, *Science*, **247**, 688 (1990).

8. C. V. Raman and Krishnan, *Nature*, **121**, 501 (1928).

9. M. G. Tobin, *Developments in Applied Spectroscopy* **Vol. 1** (Plenum Press, New York, 1962).

10. www.scimedia.com

11. N. B. Colthup, L. H. Daly, and S. E. Wilberly, *Introduction to Infrared and Raman Spectroscopy* (Academic Press, New York, 1975).

12. D. A. Long, *Raman Spectroscopy* (McGraw-Hill, New York, 1977).

13. XSI, Ann Arbor, MI.

14. Coherent, Palo Alto, CA.

15. C. Kittel, *Introduction to Solid State Physics* (John Wiley & Sons, New York, 1996).

16. Peakfit, Jandel Scientific, San Rafael, CA.

17. S. Mukamel, *Principles of Nonlinear Optical Spectroscopy* (Oxford University Press, New York, 1995).

18. P. G. Harper, and B. S. Wherret, *Nonlinear Optics* (Academic Press, London, 1977).

19. W. Zhu, G. P. Kochanski, S. Jin, and L. Siebles, J. Vac. Sc. Technol. B **14**, 2011 (1996).

20. K. H. Park and S. Lee, *J. Vac. Sc. Technol. B* **16**, 724 (1998).

21. N. M. Miskovsky, P. H. Cutler, and Z. H. Huang, *J. Vac. Sc. Technol. B* **14**, 2037 (1996).

22. J. van der Weide, Z. Zhang, P. K. Baumann, M. G. Wensell, J. Bernholc, and R. J. Nemanich, Phys. Rev. B **50**, 5803 (1994).